2023 DRAGON 5 SYMPOSIUM

3rd YEAR RESULTS REPORTING

11-15 SEPTEMBER 2023

PROJECT ID. 59197

Utilizing Sino-European Earth Observation Data towards Agroecosystem Health Diagnosis and Sustainable Agriculture

<WEDNESDAY, 13/SEPT/2023>

ID. 59197

PRINCIPAL INVESTIGATORS:

Dr. Carsten Montzka, Forschungszentrum Jülich (IBG3)

Dr. Liang Liang (梁亮), Jiangsu Normal University

Linking Agroecosystem Monitoring with Carbon Farming through Multi-Source Remote Sensing Observations

Bagher Bayat, Shuguo Wang, Carsten Montzka, Liang Liang, Jordan Steven Bates, Wensong Liu, David Mengen, Wenqin Huang, Shirin Moradi, Yuquan Qu, Rahul Raj, Visakh Sivaprasad, Renmin Yang, Lijuan Wang, Chunfeng Ma

Outline

- Background and objective
- Mid-term results
- Conclusion and outlook
- Young scientists
- EO data delivery

Background and objectives

SUSTAINABLE DEVELOPMENT GOALS

2 ZERO HUNGER

- Agriculture production systems are facing unprecedented challenges.

- EO is already used to estimate land surface variables, but the step to a full process understanding of agricultural systems has not yet been taken.

The overall objective:

To carry out **agro-ecosystem health diagnosis** and to **investigate agricultural processes** based on various in situ and EO data, allowing to improve the efficiency in the use of natural resources to facilitate **sustainable agriculture development**.

Remote sensing (multi-sensor and multi-scale)

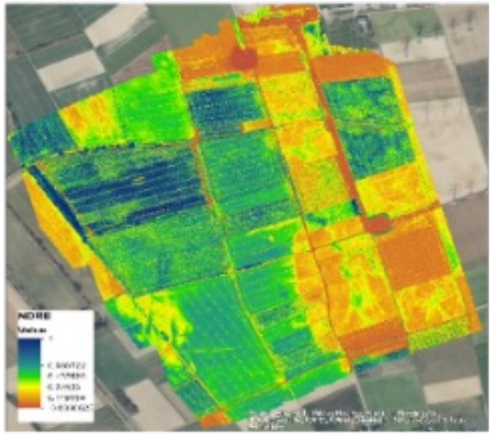

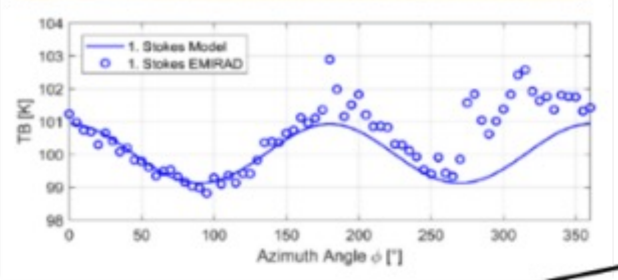

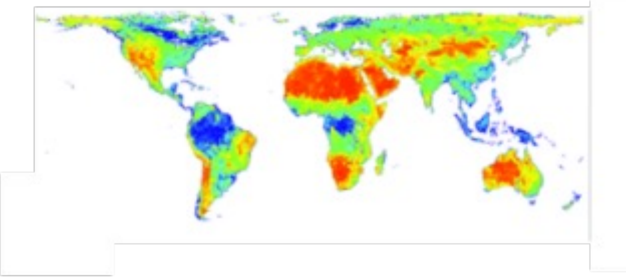

Local

Regional

Global

Scientific approach and goals

•**Development** and improvement of information **products** from remote sensing
•**Validation** of information products using in situ data
•**Integration** of information products using data **assimilation methods** and **physically-based models**

⇒**Process chain from basic data analysis to application**

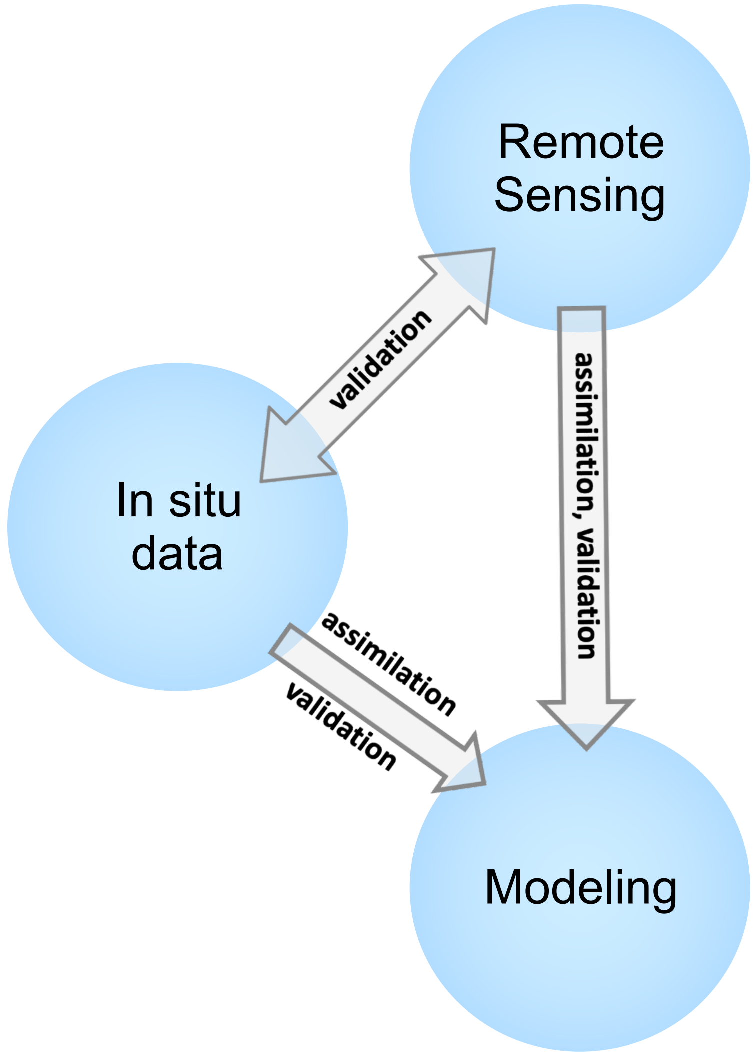

Adopted approach and workflow

The proposed workflow to support sustainable agricultural production within Dragon 5 project:

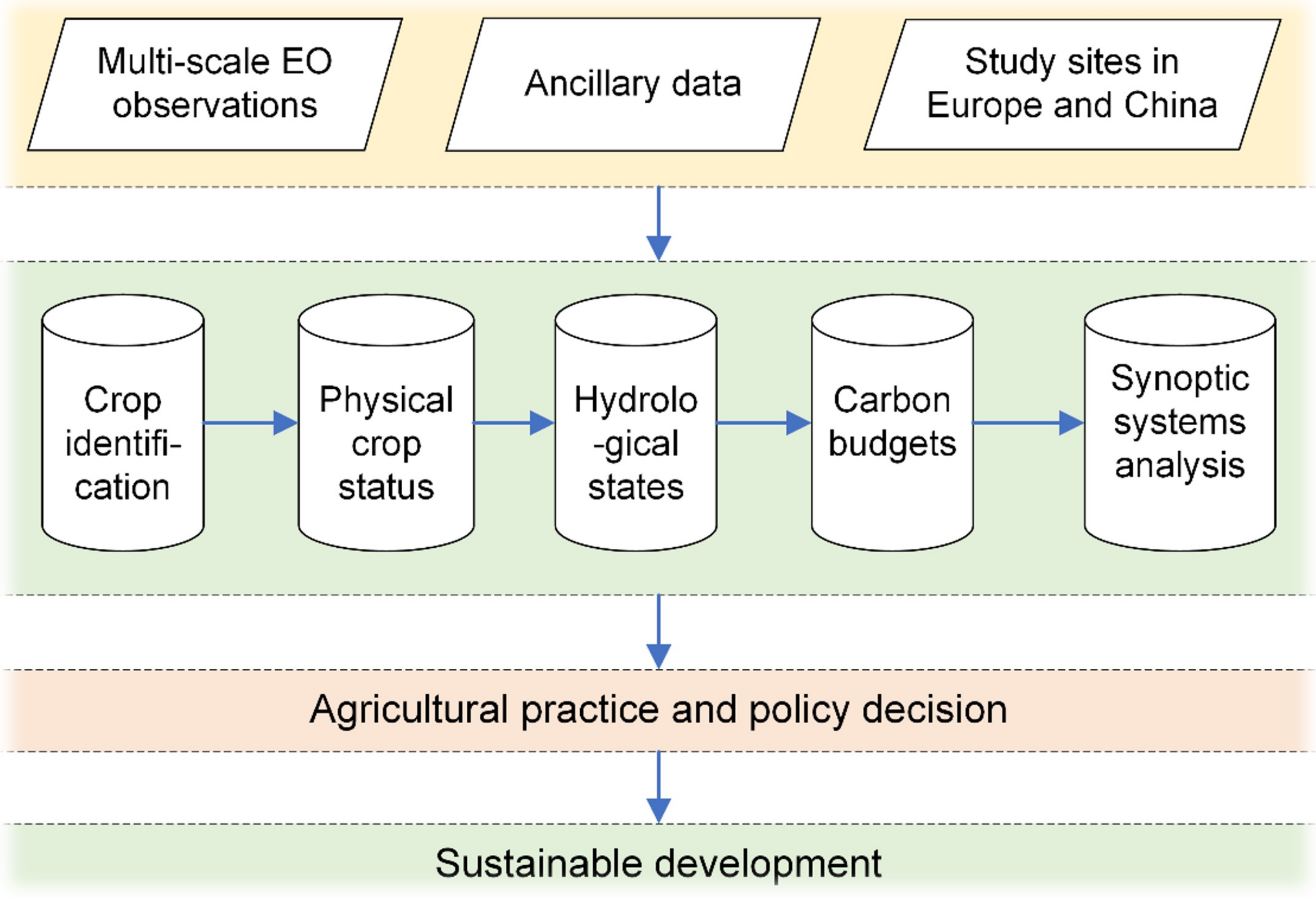

Mid-term results

European cases

1. UAV LiDAR & Multispectral LAI
2. UAV-based ET estimation
3. C&L band Soil Moisture estimation
4. Coupled modelling of soil moisture
5. RS soil moisture products comparison
6. Agricultural water stress detection
7. PlanetSCOPE & Sentinel-2 GPP

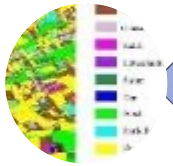

2.1 Crop identification

2.2 Observing the crop status

2.3 Observing the hydrological states

2.4 Carbon budgets

Chinese cases

1. Fusion of PolSAR & pan. images
2. UAV & Satellite Hyperspectral LAI
3. PLMR Soil Moisture estimation
4. Drought events monitoring
5. Soil organic carbon
6. Large scale NEP

UAV LiDAR & Multispectral LAI 1

Methods:

- Use LiDAR gap fraction to estimate canopy density
- Similar method to hemispherical cameras used in forestry
- Modified Beer-Lambert equation to relate laser rate of penetration to LAI

$$GF = \frac{n_{ground}}{n}$$

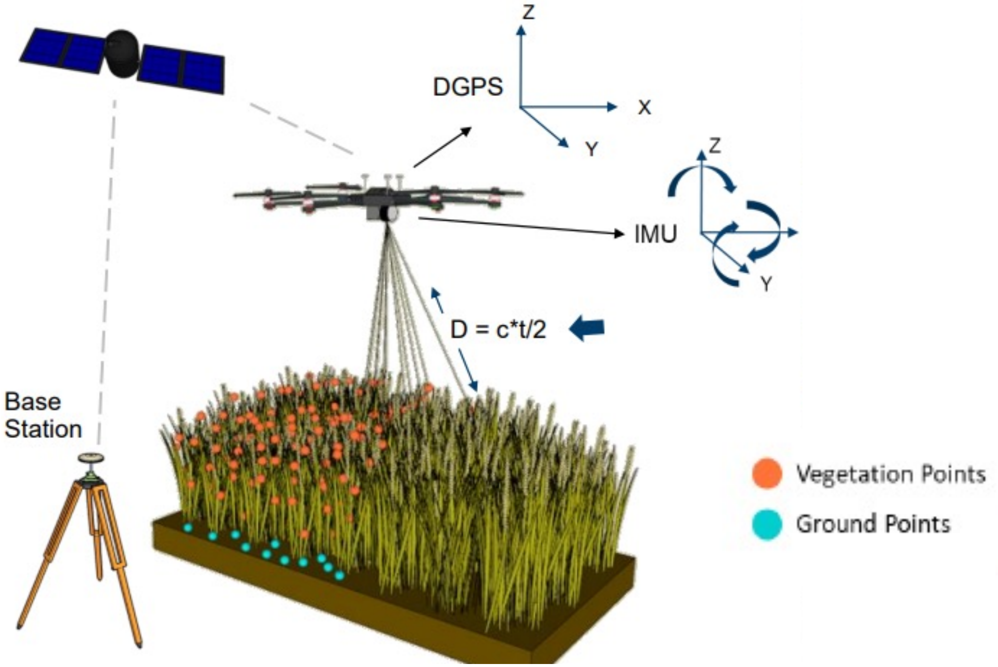

$$PAI_{LiDAR} = -\frac{\cos(\bar{\theta}) \times In(GF)}{k}$$

Modified Beer-Lambert Equation

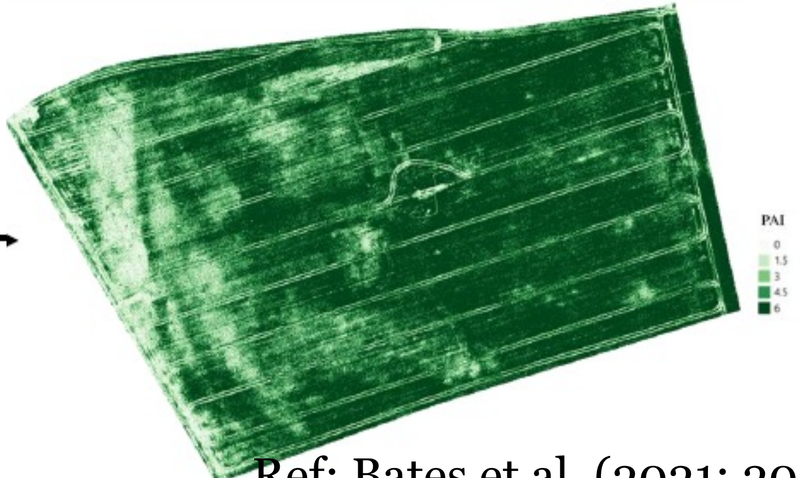

Ref: Bates et al. (2021; 2022b)

UAV LiDAR & Multispectral LAI 2

Results:

- UAV LiDAR LAI well correlated with multispectral methods (R = 0.39–0.66) and for one time destructive measurements (R2 = 0.89, RMSE = 0.89)

- Approach on PAI LiDAR and GAI multispectral methods allowed for hybrid estimation of Brown Area Index (BAI)

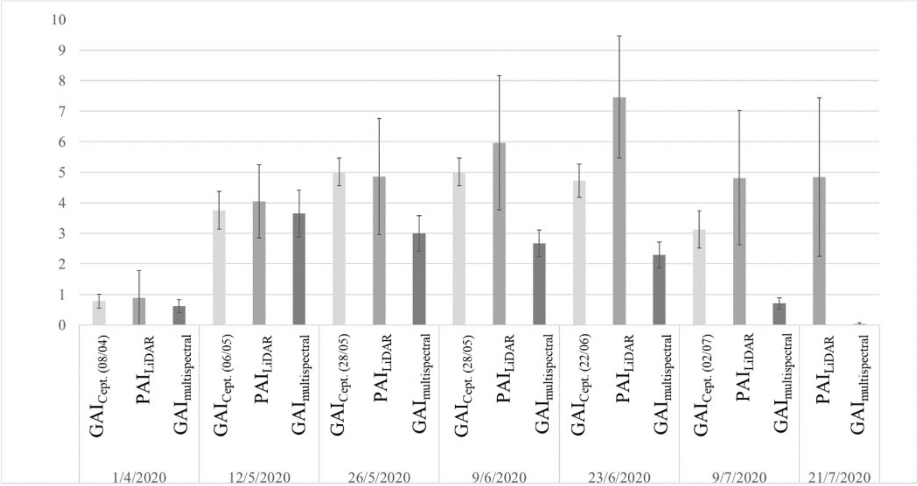

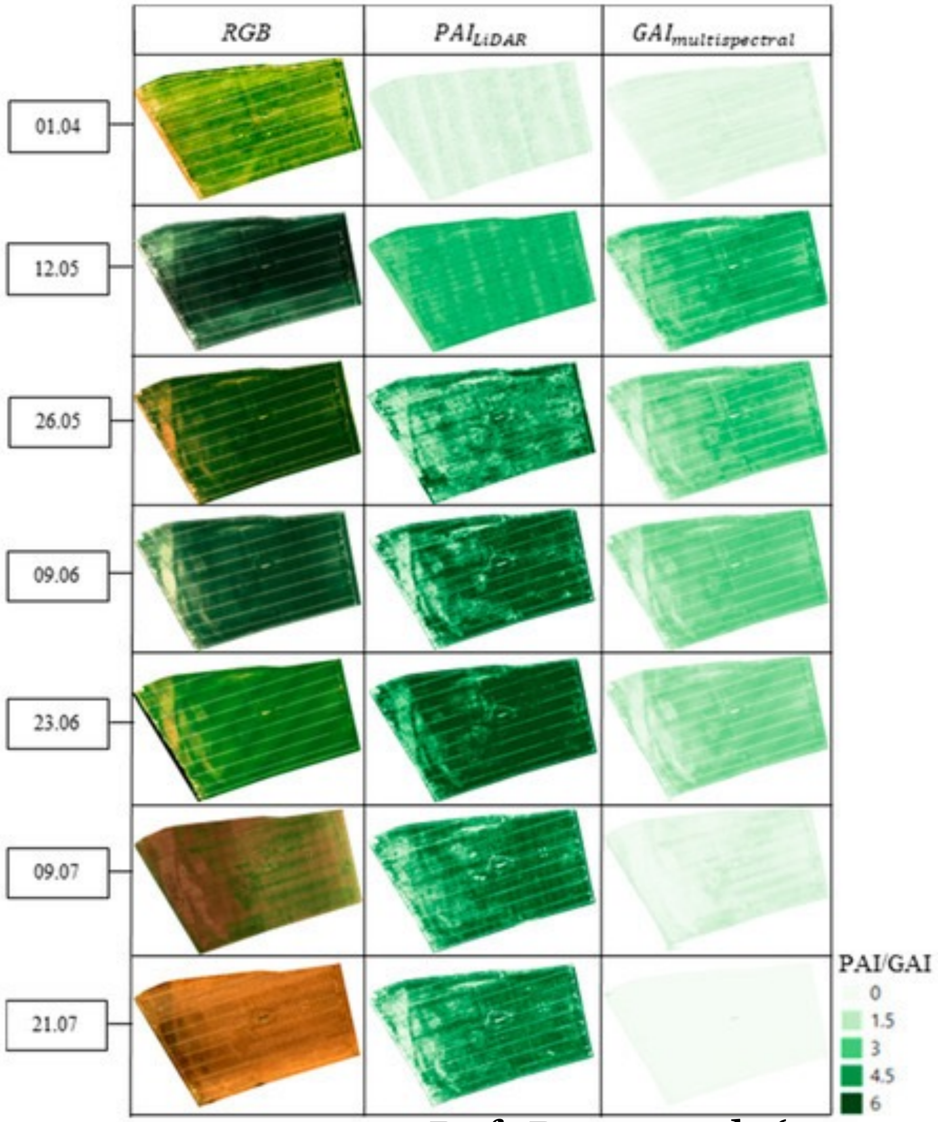

Ref: Bates et al. (2021; 2022b)

Methods for ET multi-Sensor

- Improve spatial resolution of ET for improved irrigation planning
- Use of UAV thermal sensor for Canopy and soil temperatures
- Multispectral LAI and LIDAR height for canopy and soil resistance parameters.

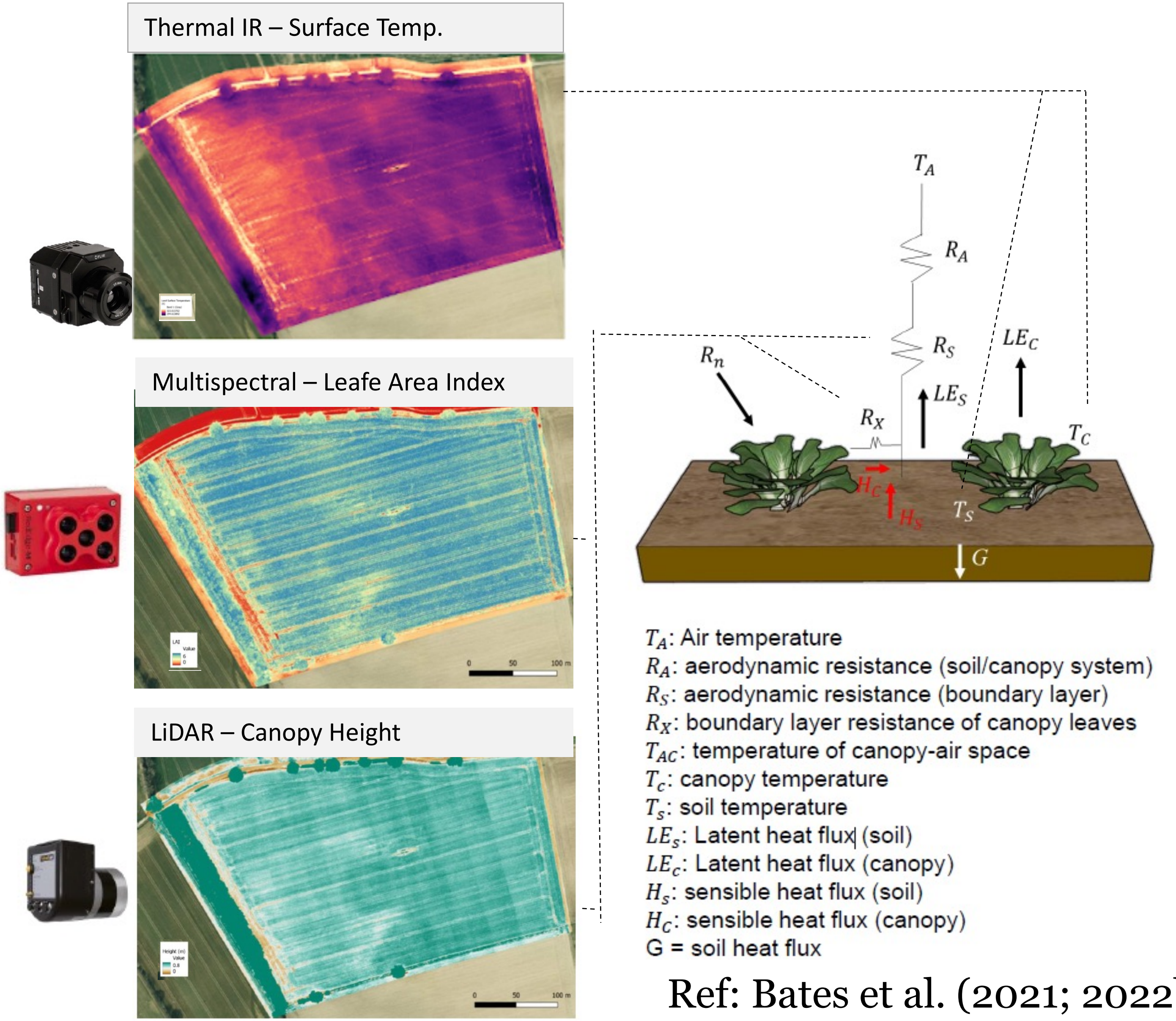

Ref: Bates et al. (2021; 2022b)

UAV-based ET estimation 2

Results

6/11/2021

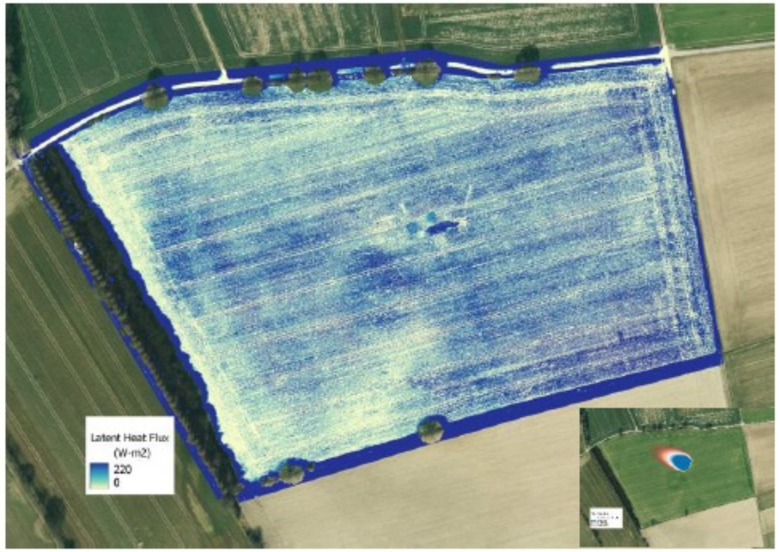

6/25/2021

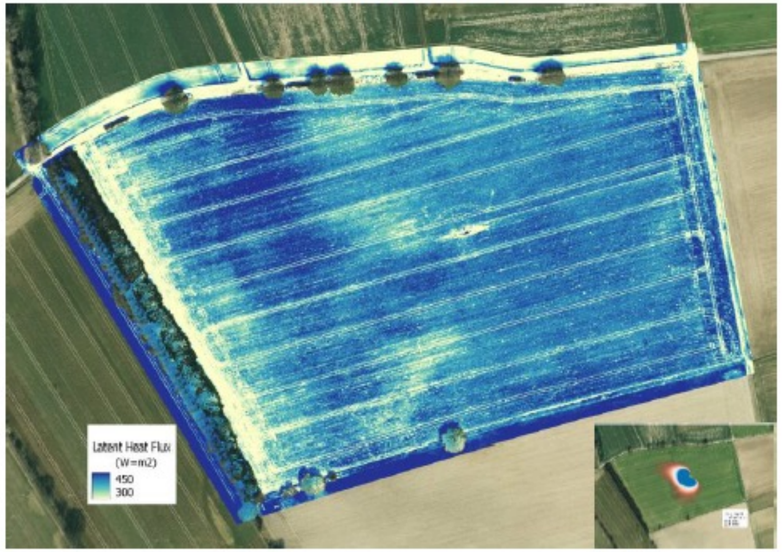

7/09/2021

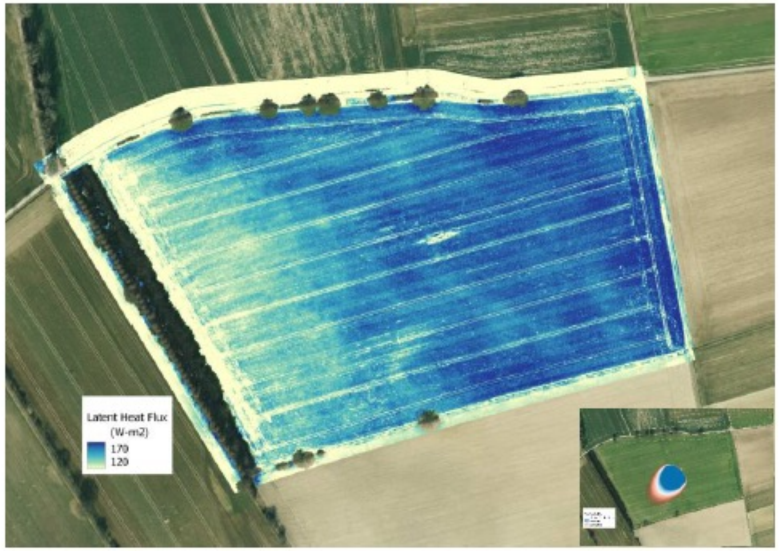

6/11/2021

Flux	EC (W-m2)	Drone (W-m2)
Net	506.43	538.3
Sensible	188.77	263.5
Latent	162.43	149.72
Soil	124.44	124.06

6/25/2021

Flux	EC (W-m2)	Drone (W-m2)
Net	637.49	599.16
Sensible	71.86	94.62
Latent	327.05	347.54
Soil	66.67	84.58

7/09/2021

Flux	EC (W-m2)	Drone (W-m2)
Net	185.72	157.68
Sensible	10.05	1.37
Latent	120.82	154.77
Soil	35.75	14.99

TSEB-PT Model

Latent Heat Flux

Overall RMSE: 11.83

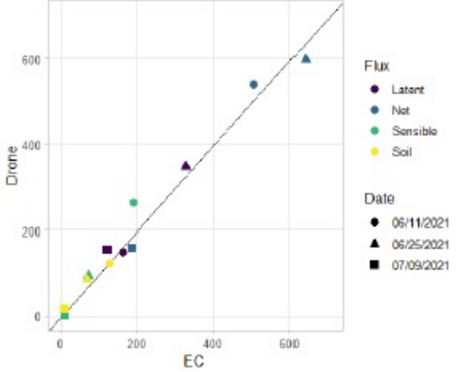

Ref: Bates et al. (2021; 2022b)

Results

- The method has found good agreement between the latent heat fluxes of UAS TSEB and ground-based eddy covariance (EC) estimates with an RMSE of 11.83 W/m2 based on three observations earlier in the growing season.

- More complete and frequent depictions of ET allow for more responsive and precise irrigation planning that can improve water use efficiency.

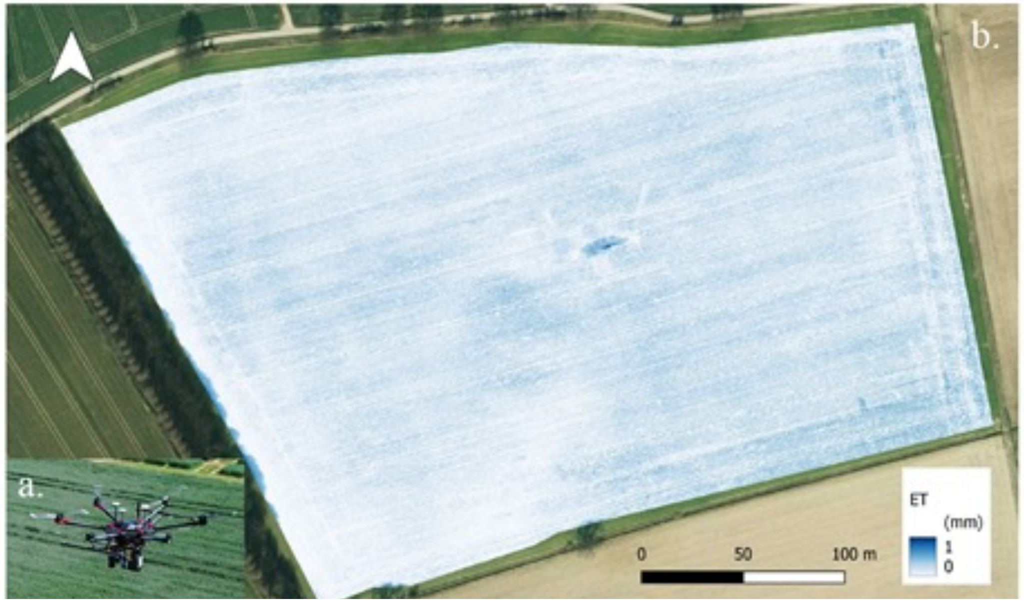

Ref: Bates et al. (2021; 2022b)

C&L band Soil Moisture estimation 1

Background

- Using a short-term change detection method, changes between SAR observations mostly related to changes in soil moisture
- C-band Sentinel-1 timeseries offers temporal dense recordings but is prone to vegetational influence
- L-band ALOS-2 timeseries is not as prone to vegetational influence but has only scattered recordings

Objective

- How to combine both timeseries to have vegetational insensitivity of ALOS-2 L-band with high temporal resolution of Sentinel-1 C-band?

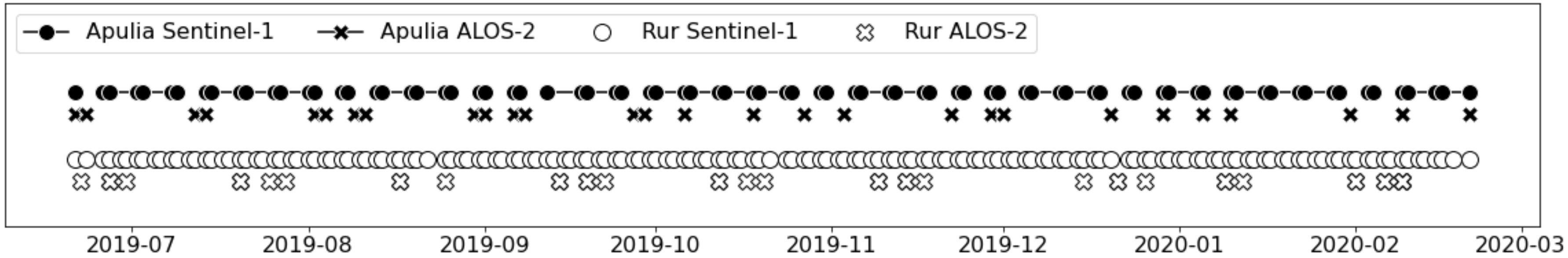

Ref: Mengen et al. (2023)

Method

- Changes in the L-band are less influenced by vegetation and serve as "reference points“
- Between observations in the L-band, the time series in the C-band are scaled to match the observed scenes in the L-band
- Soil texture is used for inverting soil moisture to dielectric constant

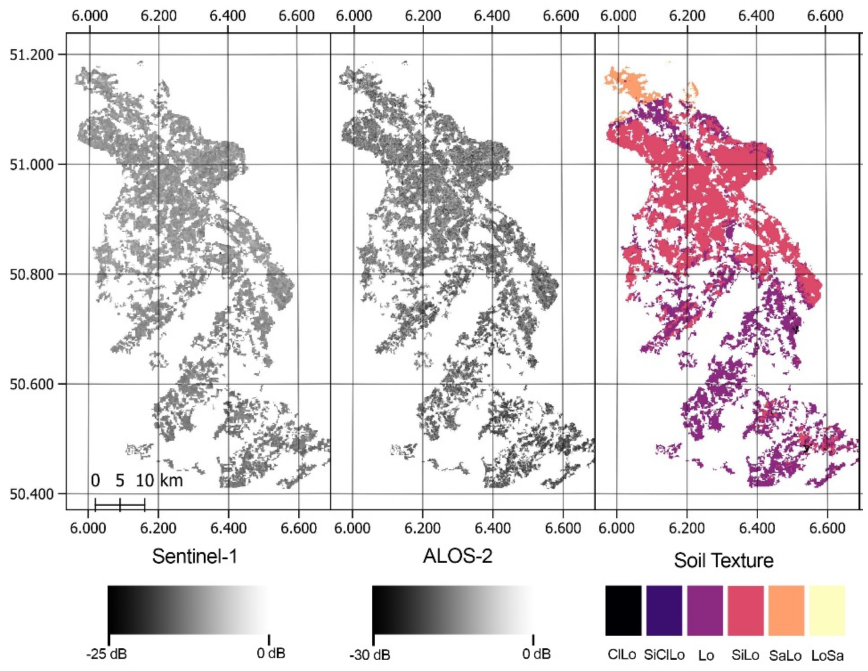

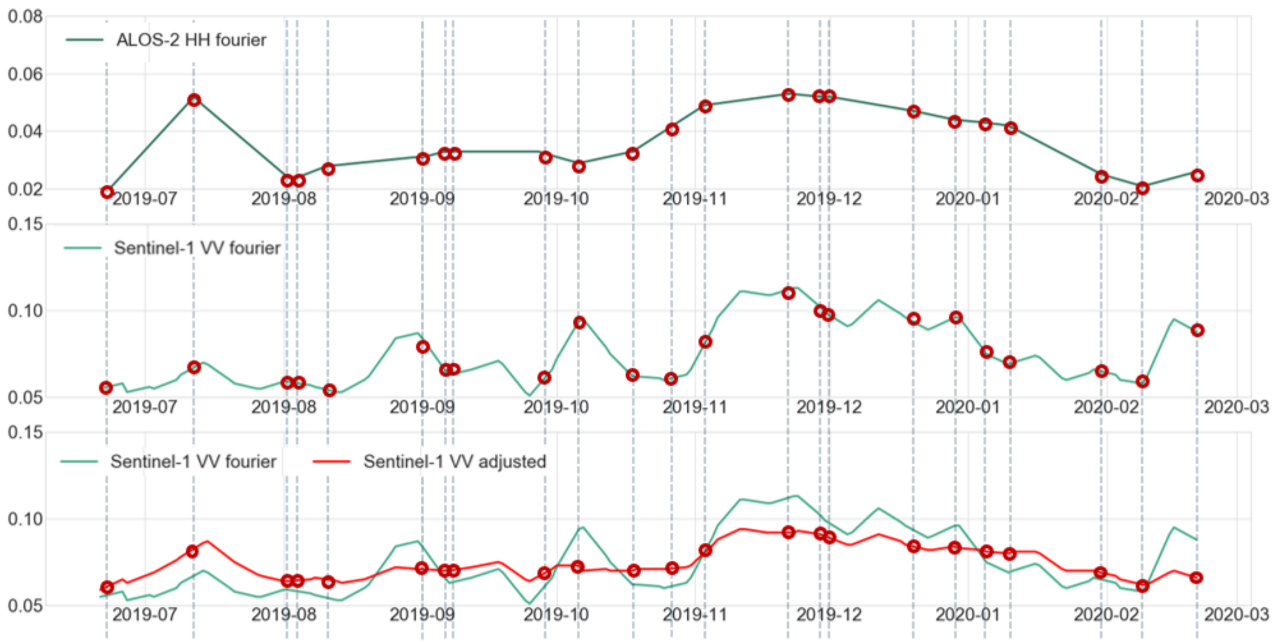

Ref: Mengen et al. (2023)

C&L band Soil Moisture estimation 3

Results

- Soil moisture estimation from Alos-2 matches in-situ measured soil moisture better in absolute terms, but sparse temporal resolution leads to lack of correlation

- Soil moisture estimation from Sentinel-1 has higher correlation but also higher absolute error

- Soil moisture estimation from both C- and L-band combines higher correlation and lower absolute error

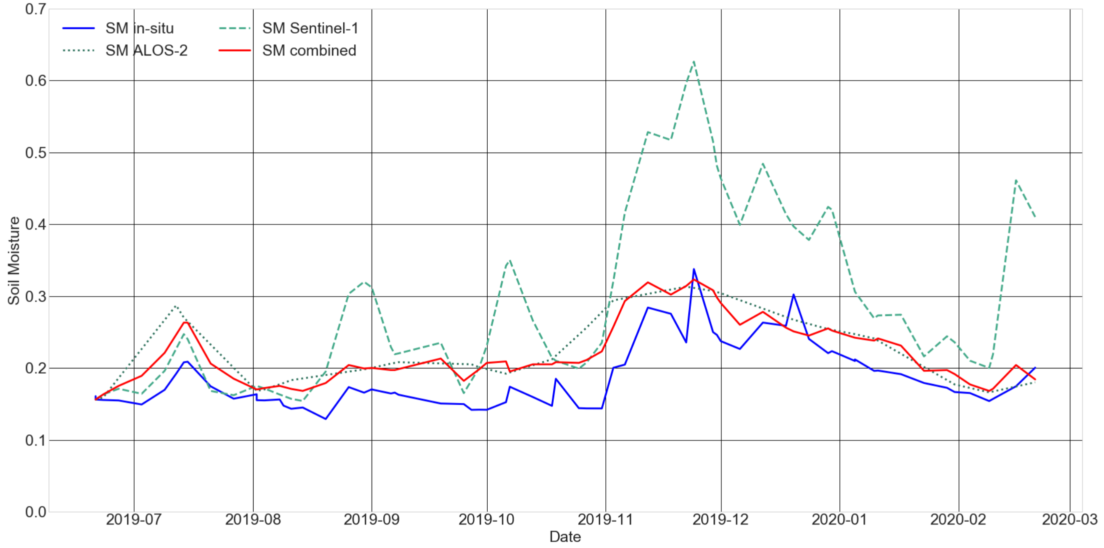

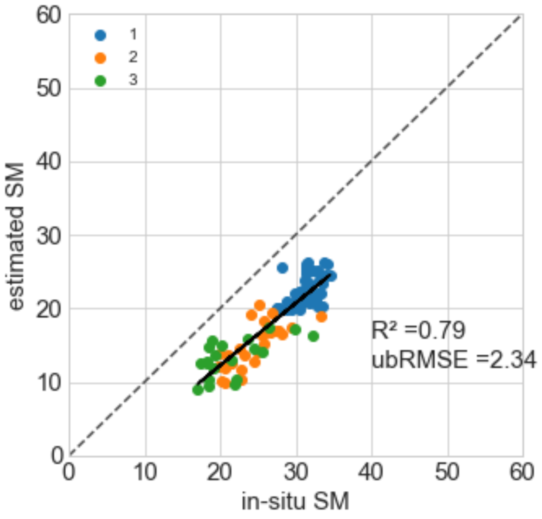

Barley

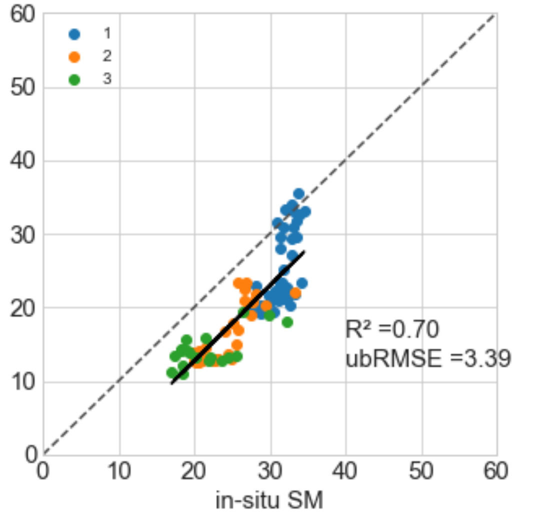

Wheat

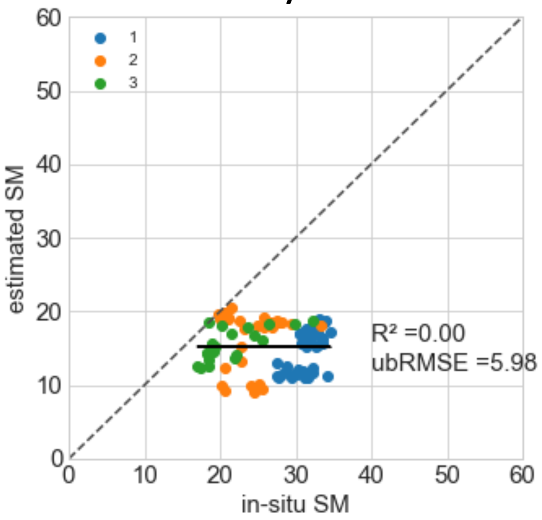

Sugar Beet

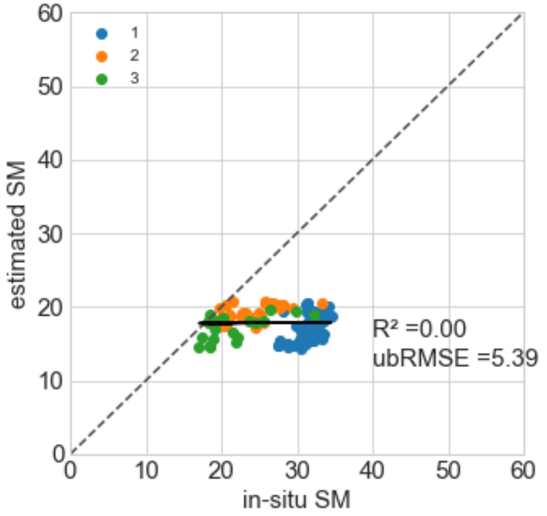

Potato

Ref: Mengen et al. (2023)

C&L band Soil Moisture estimation 4

Results

- Significant improvement in linear, upright crops (wheat, barley).

- For taproot or tuber crops such as potatoes and sugar beets, the change in surface roughness due to maturity and harvest becomes a challenge for combined C- and L-band change detection methods.

- Apply combined C- and L-band change-detection method for stationary surface roughness conditions within L-band wavelength domain -> between seeding and harvest

White areas excluded==> water, urban and Forest
Blue ==> wet
Orange ==> dry
Resolution==> 200 m and 2 days

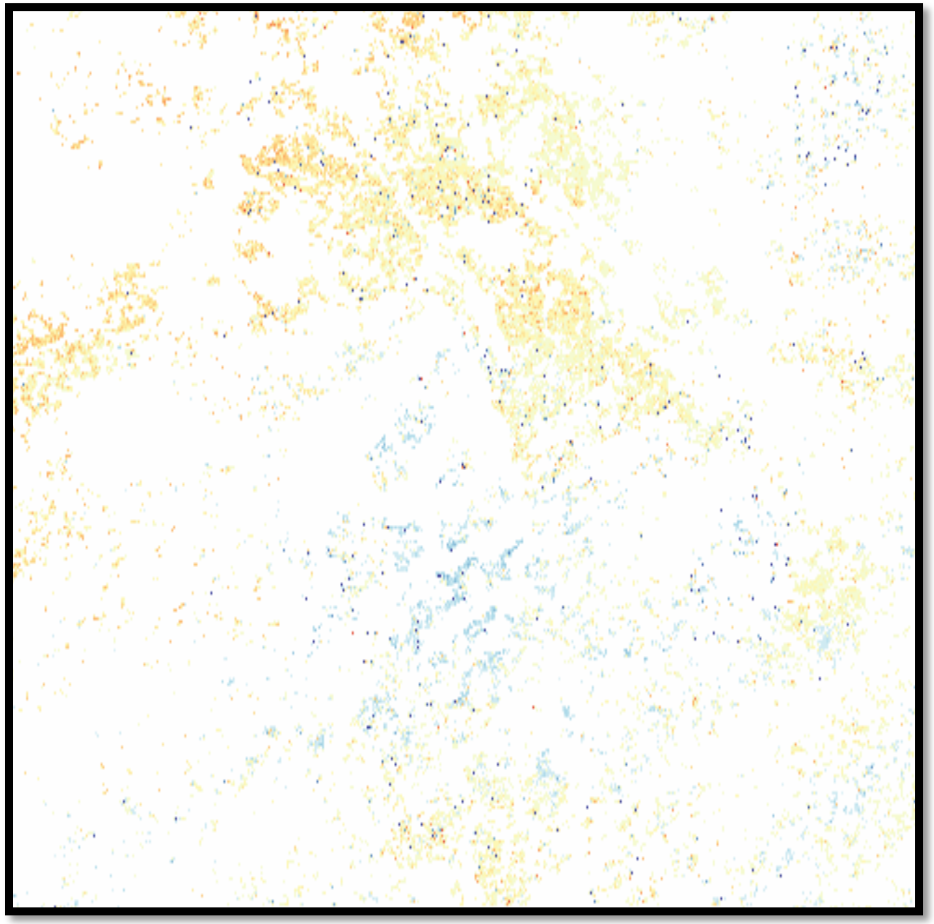

Ref: Mengen et al. (2023)

Coupled modeling of soil moisture 1

Methods

- Coupled land surface-subsurface model (CLM-ParFlow).
- 500m resolution
- Meteorological forcing: COSMO-REA6 2017-8 (normal & dry year)
- Soil hydraulic properties: Rosetta Pedo-transfer functions.
- Soil texture: FAO/UNESCO Soil Map (Klimaatlas NRW)
- Water retention and relative permeability curves: the van Genuchten

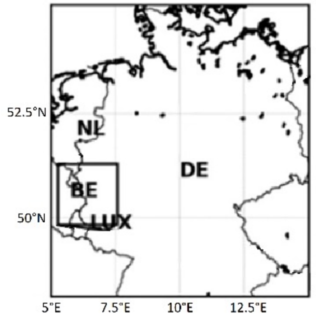

Study area (150 km^2)

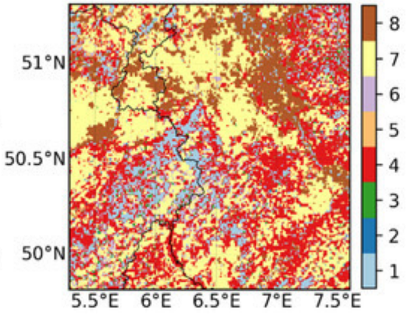

The plant functional types (PFTs): MODIS land cover data

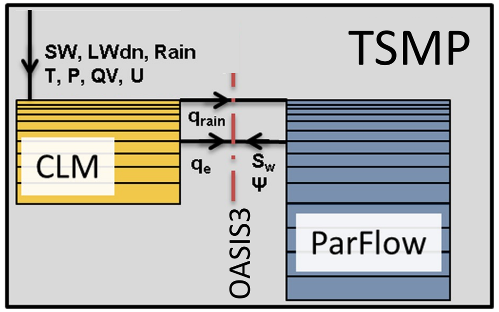

From Shrestha et al. 2014

Ref: Moradi et al. (202X)

Coupled modeling of soil moisture 2

Results:
Simulated vs Measured Soil Moisture …

Cross-evaluation of Simulated SM
- Cosmic-ray neutron sensor (CRNS) (13 stations)
- Soil Moisture Active/Passive (SMAP)
- Synthetic Aperture Radar (SAR)-Sentinel-1

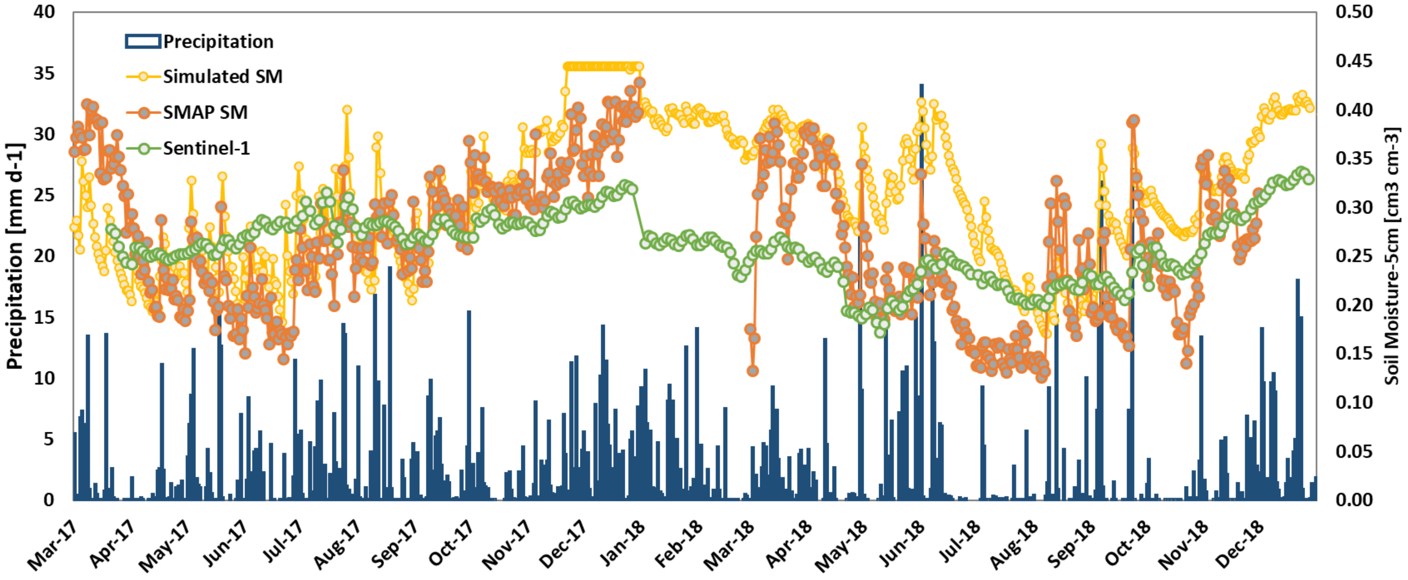

Variation in the simulated vs SMAP and Sentinel-1 extracted SM of the top 5cm of the soil and the precipitation at the study area for 2017-8

Mean Monthly	bias	RMSE	ubRMSE	r
CRNS	-0.02	0.15	0.11	0.38
SMAP*	0.04	0.01	0.05	0.48
Sentinel1	0.06	0.01	0.07	0.45

* Resolution difference is not considered : 0.5 km vs 9

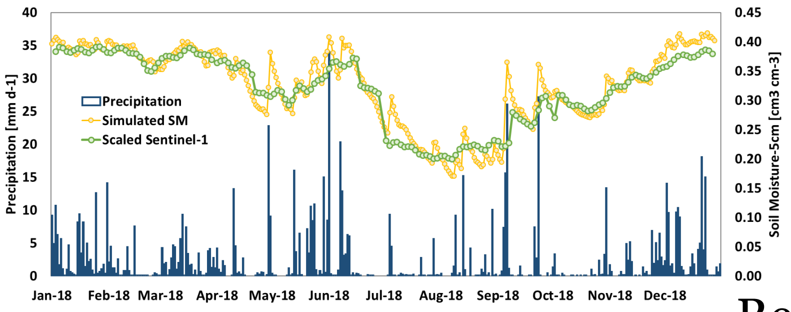

Ref: Moradi et al. (202X)

Coupled modeling of soil moisture 3

Results & Outlook

- The model is able to capture the SM values and dynamics to some extent.
- Relatively low systematic bias (ubRMSE)
- SM dynamics are best captured when precipitation is more steady
- Relatively low correlation values at 500m resolution

Next:

- Data assimilation towards improving the simulation results using high resolution satellite data.

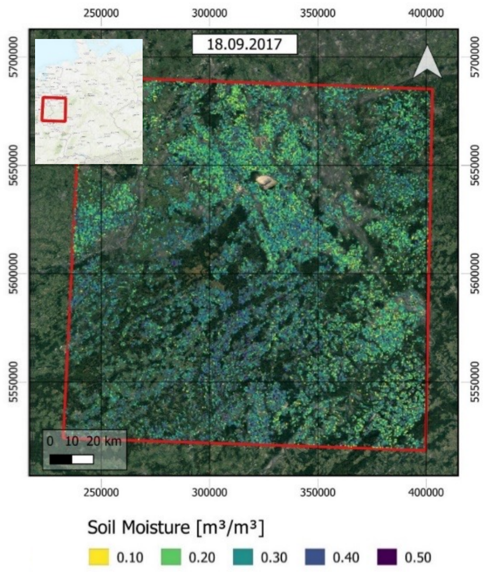

SM from Sentinel-1 for September 2017

Ref: Moradi et al. (202X)

RS soil moisture products comparison 1

Methods:

- The analysis was conducted at the TERENO-Rur site network in Germany for years from 2016 to 2018.
- The in-situ soil moisture, from the ISMN (International Soil Moisture Network) database, served as the benchmark.
- To ensure consistency, the hourly volumetric soil moisture (in-situ) at a depth of 5cm were averaged to daily.

Different preprocessing approaches: a) smoothing, b) scaling, c) gap filling

DATA	Detail	Processing level	Bands	Latency	Spatial resolution	Temporal resolution	Coverage
SMAP	Soil Moisture Active Passive	L3	L-band	31 March 2015 to present	36*36 km	Daily	Global
AMSR-E	Advanced microwave scanning radiometer – Earth observation system	L3	C, X-band	2002-06-19 to 2011-10-04	25*25 km	Daily	Global
AMSR-2	Advanced microwave scanning radiometer - 2	L3	C, X-band	2012-03-07 to till date	25*25 km	Daily	Global
SMOS	Soil moisture ocean salinity	L3	L band	2015-05-06 to 2022-07-31	25*25 km	Daily	Global
ESA CCI	Climate Change Initiative	L3		1978 to 2021	25*25 km	Daily	Global
ASCAT	Advanced Scatterometer	V7	C band	2007-01-01 to till date	12.5*12.5 km	Daily	Global

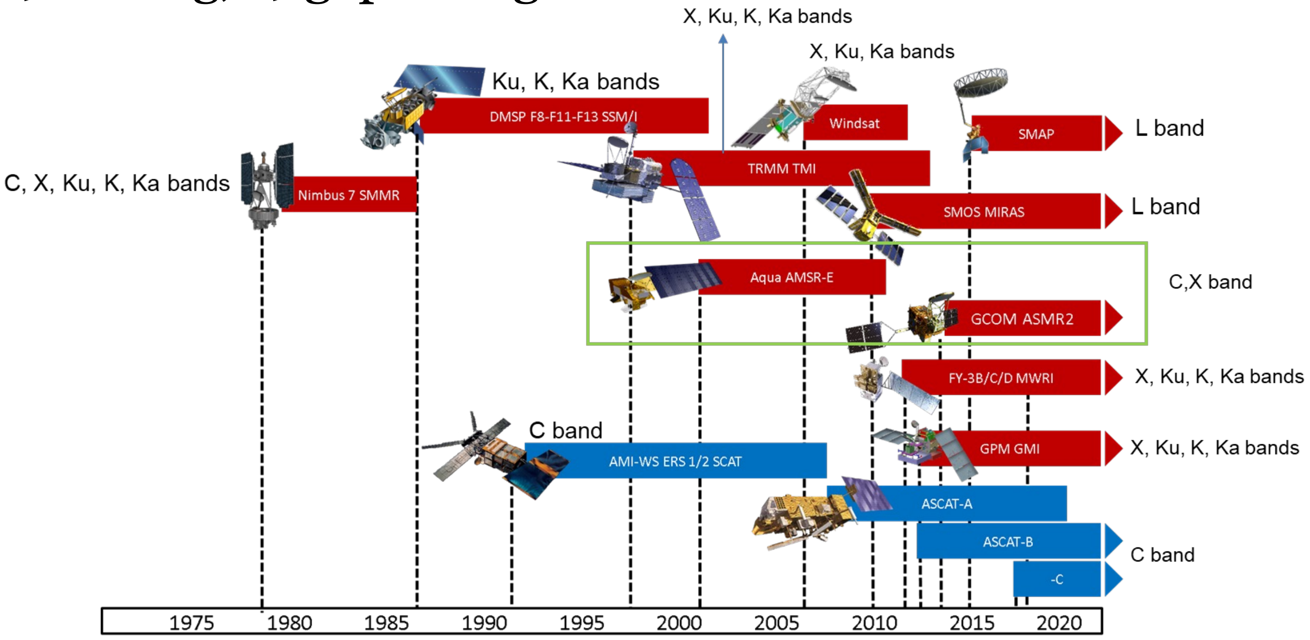

Ref: Sivaprasad et al. (202X)

RS soil moisture products comparison 2

Smoothing and Scaling:

- SMAP shows the best performance across evaluation metrics followed by ESA-CCI.
- Smoothing improved the performance of AMSR2
- Scaled AMSR2 data effectively captures the dynamics of SMAP.
- SMAP and Scaled-AMSR2 also demonstrate relatively strong performance.

AGRICULTURAL SITE (GEVENICH)

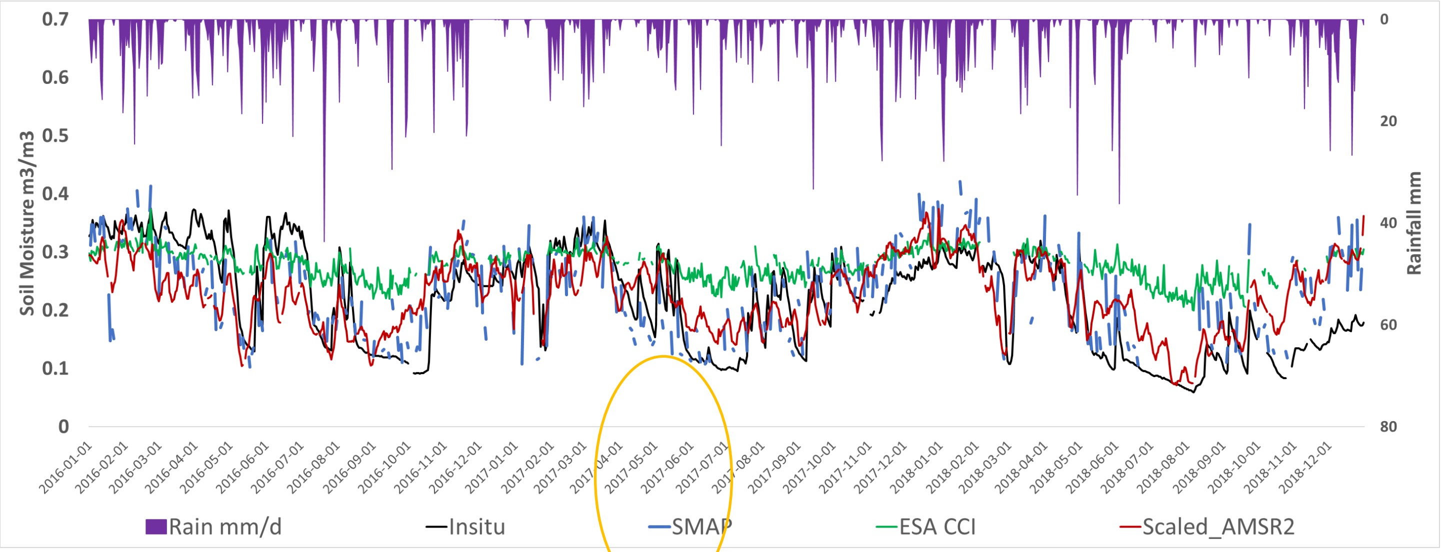

	Pearson's R	Spearman's rho	Kendall's tau	RMSE	Bias	ubRMSE
SMAP	0.714	0.723	0.528	0.06	0.007	0.06
ESA CCI	0.831	0.837	0.635	0.091	0.058	0.069
AMSR2_SAVGOL	0.669	0.658	0.456	0.08↓	0.048↓	0.064
SMOS_SAVGOL	0.55	0.589	0.417	0.092	-0.07	0.06
ASCAT_SAVGOL	0.406	0.398	0.268	0.107	0.068	0.083
Scaled_AMSR2	0.669	0.658	0.456	0.065↓	0.009↓	0.064

Ref: Sivaprasad et al. (202X)

RS soil moisture products comparison 5

Results:
Gap filling

- Compared to all data, SMAP performs better. But for long term data assimilation, better to have long term continuous dataset.
- AMSR-E/AMSR-2 data is available from 2002 to 2022, but with a gap of 7 months.
- Random forest ML is used here to fill the gap between AMSR-E and AMSR-2 data.
- Ancillary data: ASCAT, SMOS, soil texture, day of the year were used as the inputs to predict.
- Verification was done with the AMSR2 and In-situ data.

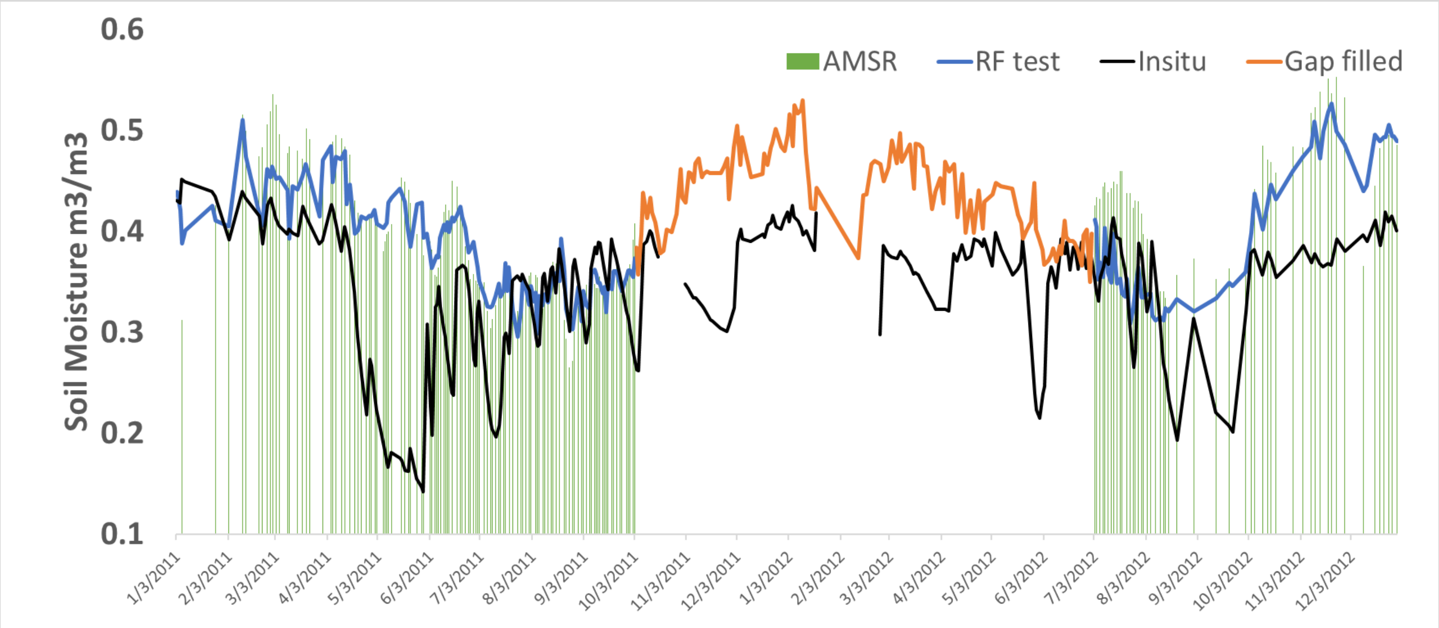

Pearson's R	0.841
Spearman's rho	0.811
Kendall's tau	0.629
RMSE	0.039
Bias	-0.016
ubRMSE	0.035

Ref: Sivaprasad et al. (202X)

Results:

- We found that SMAP generally outperformed other satellite products in representing soil moisture.

- SMAP fell short in meeting the long-term time series requirements. We explored AMSR-E/2 as an alternative with a longer time series but limited accuracy.

- Through the application of the Savitzky-Golay filter and scaling with respect to SMAP, we achieved improved performance across all land covers. Additionally, employing the Random Forest algorithm for gap filling showed promising results.

Ref: Sivaprasad et al. (202X)

Agricultural water stress detection 1

Methods:

- Accuracy assessment of daily SEVIRI-ET_a and SEVIRI-ET_0 products (2004-2018) against in situ measurements at 54 eddy covariance sites
- Accuracy separation into temporal (intra-annual and inter-annual) and spatial (ecosystem, and climate zones) dimensions
- Water stress levels detection for the entire Europe for 2004-2018 at 3 km resolution

$$\mathrm{KGE} = 1 - \sqrt{(r-1)^2 + \left(\frac{\sigma_s}{\sigma_g} - 1\right)^2 + \left(\frac{\mu_s}{\mu_g} - 1\right)^2}$$

$$ESI = \frac{ETa}{ET0}$$

$$< ESI(d,y,i,j) > = \frac{1}{nc} \sum_{n=1}^{nc} < ESI(n,y,i,j) >$$

$$ESIA = \frac{< ESI(d,y,i,j) > - \frac{1}{ny} \sum_{y=1}^{ny} < ESI(d,y,i,j) >}{\sigma(d,i,j)}$$

r: is the linear correlation between two dataset,
σ_s: the standard deviation in satellite,
σ_g: the standard deviation in in situ,
μ_s: the satellite mean,
μ_g: the ground mean.
The ratios σ_s / σ_g and μ_s / μ_g describe the variability error and the bias term

ETa: Actual ET [mm/day]
ET0: Reference ET [mm/day]
ESI: Evaporative Stress Index [-]
ESIA: Evaporative Stress Index Anomalies [-]
d: daily time step,
y: year, i,j: grid location
nc: number of observations,
n: value of observation

Ref: Bayat et al. (2022)

Agricultural water stress detection 2

Results:

Temporal (Intra/Inter-annual)

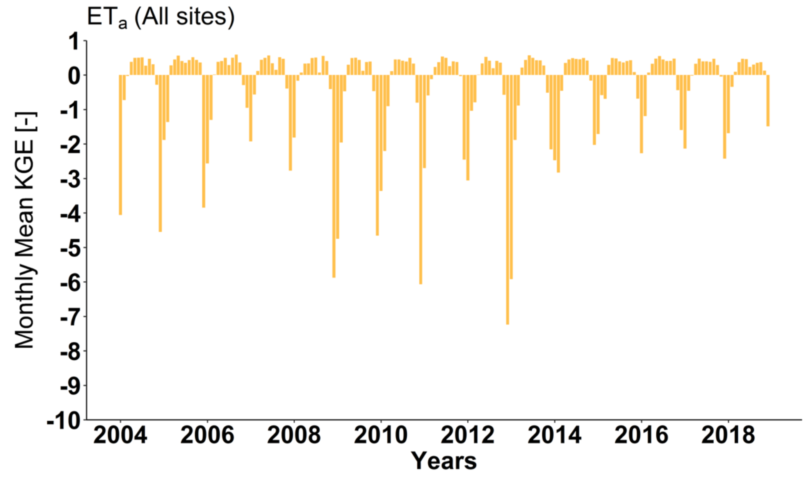

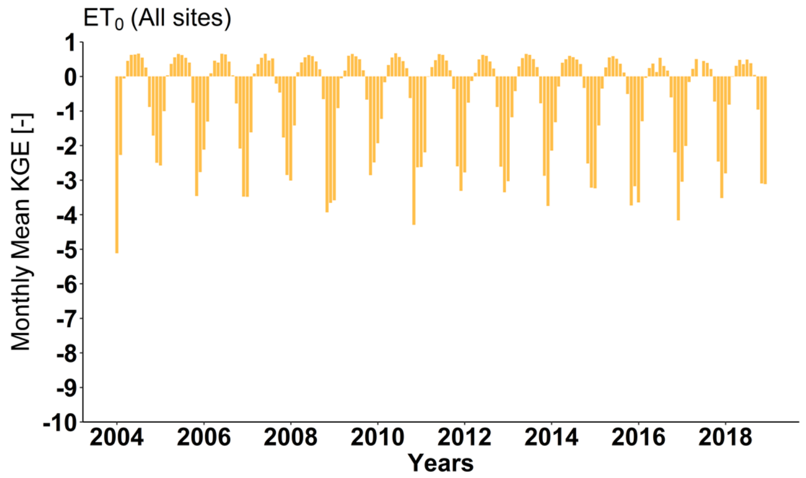

Spatial (Ecosystem)

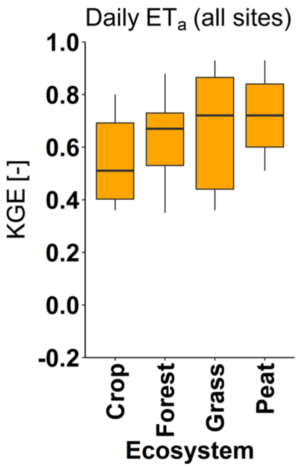

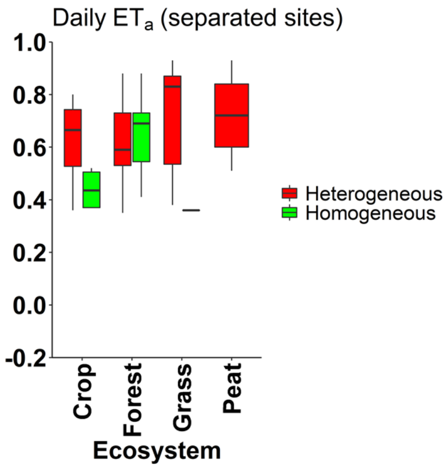

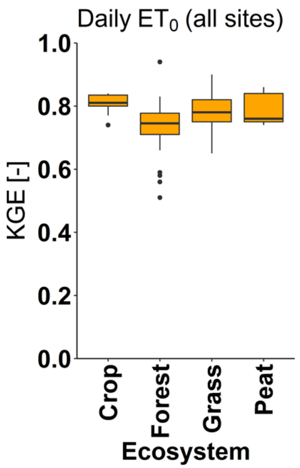

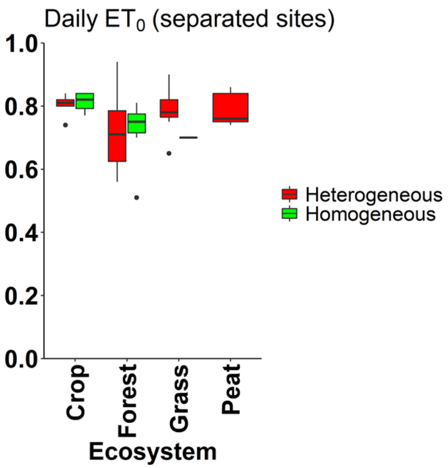

Spatial (Climate)

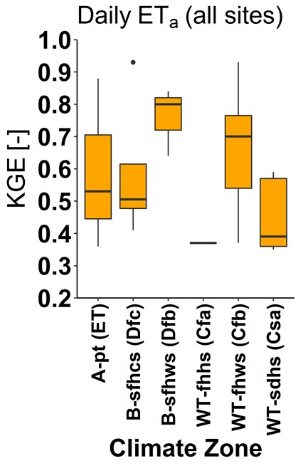

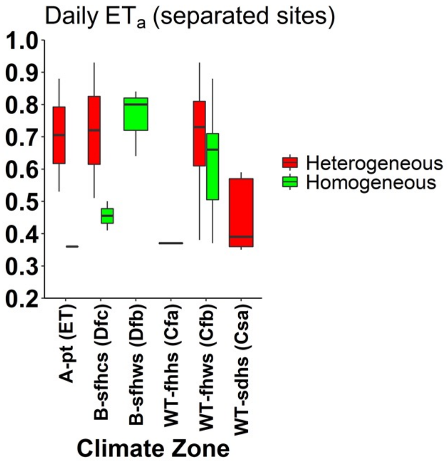

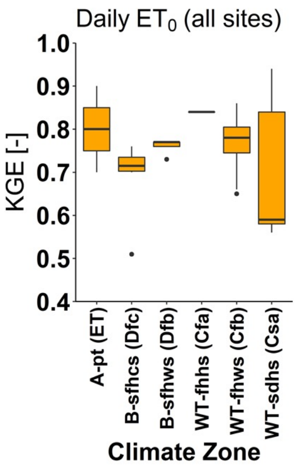

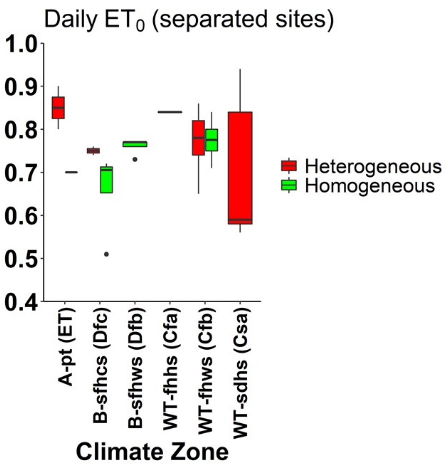

Ref: Bayat et al. (Revised for RSE)

Agricultural water stress detection 3

Results:

Water stress maps

- ✓ 3-5 km spatial resolution
- ✓ Monthly temporal resolution
- ✓ 15 years (2004-2018)

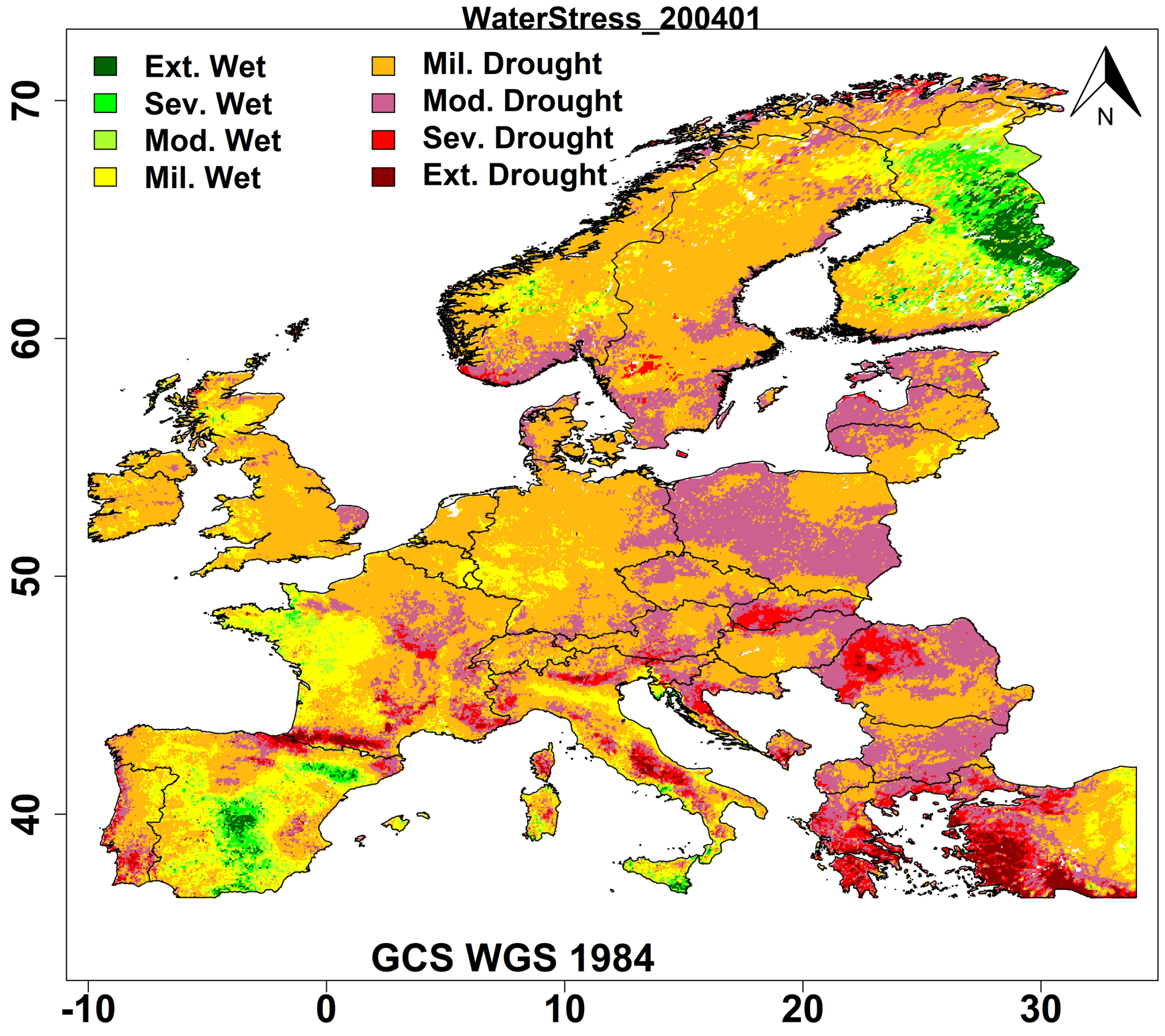

Ref: Bayat et al. (2022)

Results:

- The direct comparison of in situ ET with their corresponding SEVIRI-ET products resulted in a fair agreement in spatial dimensions albeit with expected inter-site variability.
- For SEVIRI-ET, intra-annual accuracy was low from January to March, increased in the mid-year, and then began to decline from November to December.
- The water stress workflow based on Evaporative Stress Index (ESI) anomalies can be used in operational applications to quantify various water stress levels.
- The results from this study highlight the value, support the potentials, and unlock the full capacity of SEVIRI-ET products and the VLab platform for agricultural water stress detection at larger domains.

Ref: Bayat et al. (2022)

Methods:

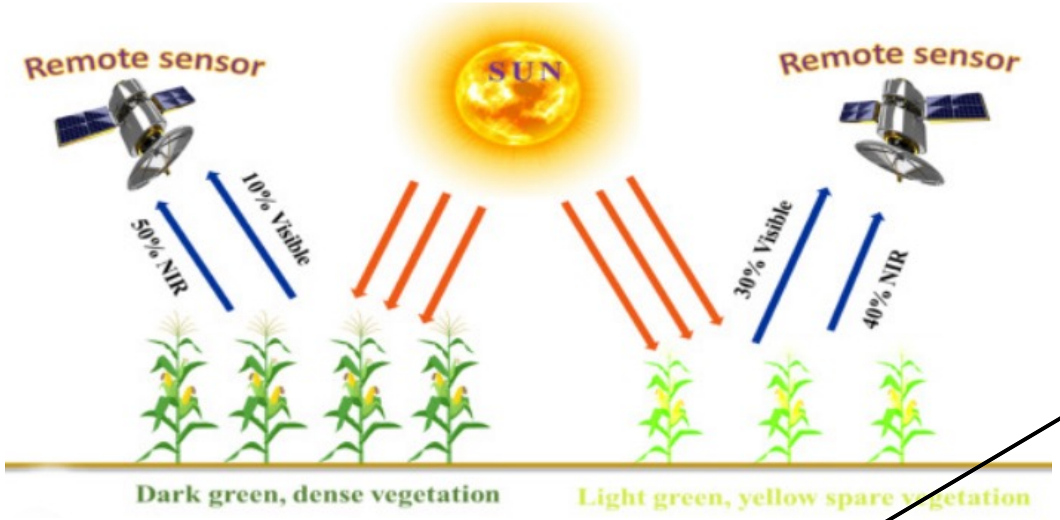

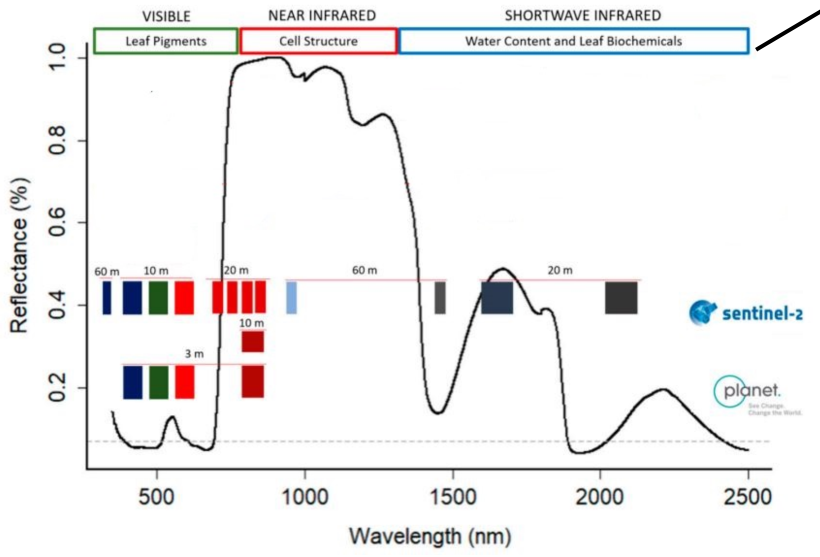

Inversion of radiative transfer model → **LAI** → **Light use efficiency model calibration and implementation** ← **Met condition (Ta, VPD)**

$$\mathbf{GPP} = \boldsymbol{\varepsilon} \times \mathbf{APAR} = \boldsymbol{\varepsilon} \times \mathbf{fAPAR} \times \mathbf{PAR}$$

Light use efficiency (ε) is calculated as:

$\varepsilon = \varepsilon_{max} \times \text{Attenuation scalars} = \varepsilon_{max} \times T_s \times W_s$

Attenuation scalars account for environmental stress on maximal light use efficiency (ε_{max})

fAPAR from LAI using Beer's Law approach:

$\text{fAPAR} = 1 - e^{(-k) \times \text{LAI}}$

$$T_s = \begin{cases} 0 & T_{min} < 0 \\ \dfrac{(T_a - T_{min})}{(T_{max} - T_{min})} & T_{min} \le T_a \le T_{max} \\ 1 & T_a > T_{max} \end{cases}$$

$$W_s = \begin{cases} 0 & VPD > VPD_{max} \\ \dfrac{(VPD_{max} - VPD)}{(VPD_{max} - VPD_{min})} & VPD_{min} \le VPD \le VPD_{max} \\ 1 & VPD < VPD_{min} \end{cases}$$

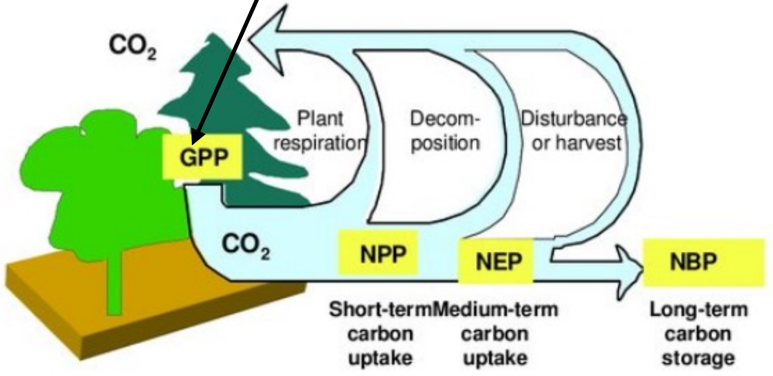

Ref: Raj et al. (202X)

PlanetSCOPE & Sentinel-2 GPP 2

Results:

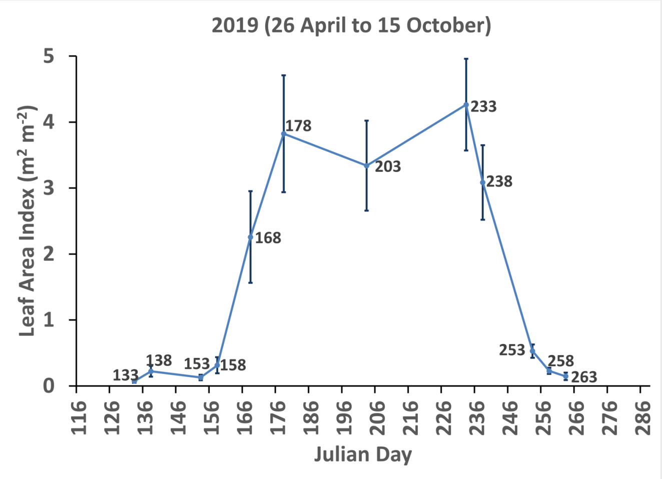

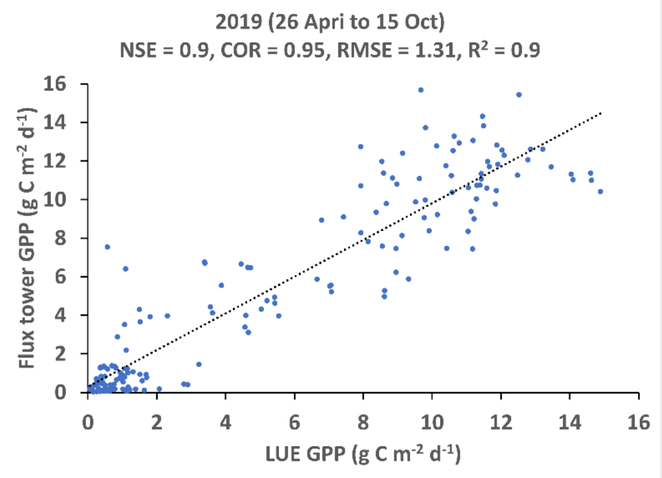

Mean retrieved LAI from Sentinel 2 (10m) and GPP from the sowing (26 April 2019) to the harvesting (15 October 2019) date of the potato crop field at the Selhausen ICOS (Integrated Carbon Observation System) site, Germany.

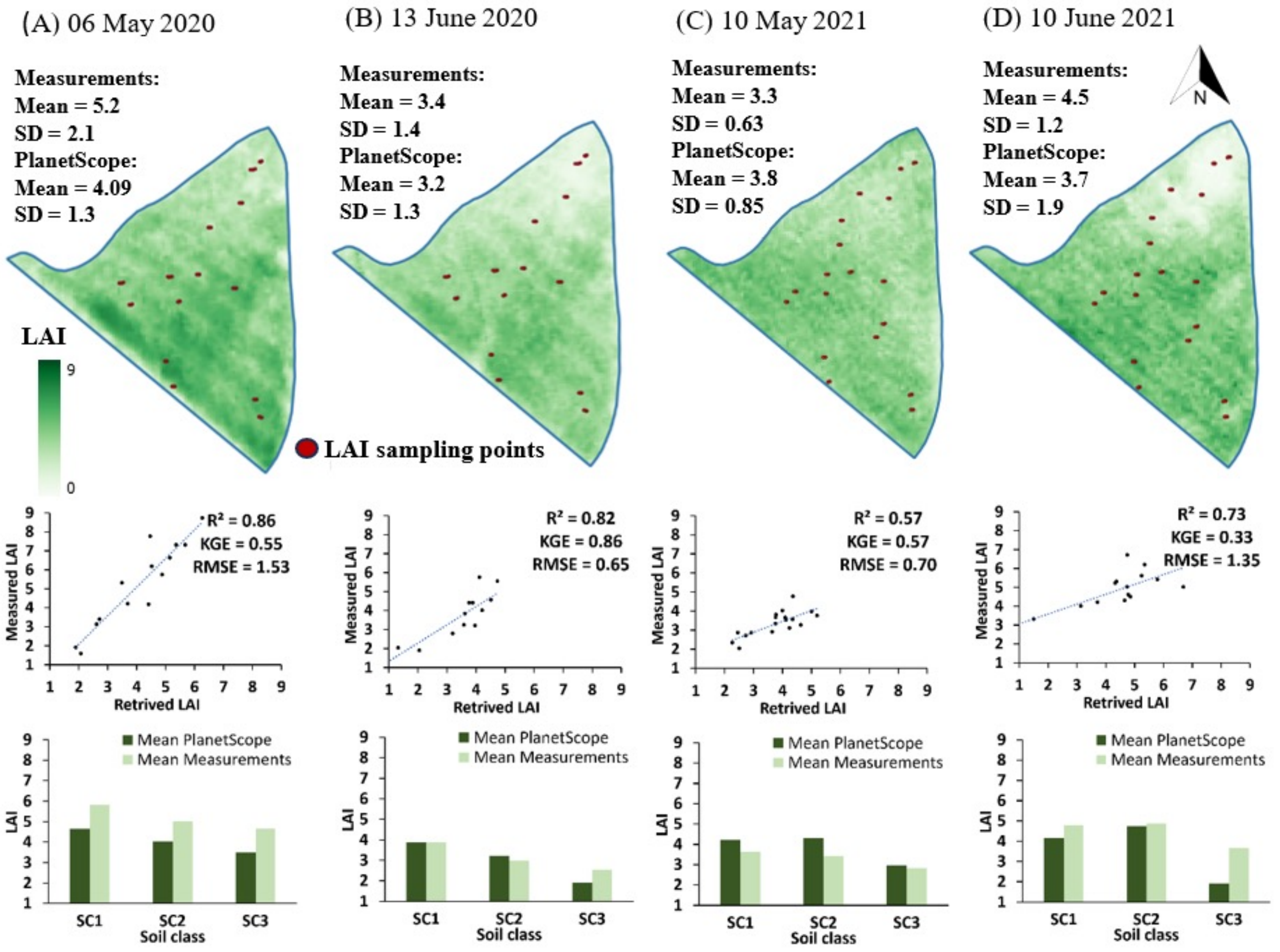

LAI retrieval from PlanetScope data (3m) for two winter triticale phenological stage (end of stem elongation and end of flowering phase) in 2020 and 2021 at Löwenberger Land, Grossmutz, Germany.

Ref: Raj et al. (202X)

Results:

- The growth development of potato and winter triticale was apparently reflected by the retrieved LAI.
- LAI retrieved from the Sentinel-2 can serve as the quality-assured estimate of crop GPP.
- LAI retrieved from PlanetScope can capture the spatial heterogeneity in LAI that results from the spatial variation in soil water holding capacity.

Ref: Raj et al. (202X)

Fusion of PolSAR & pan. images 1

- To take full advantage of high spatial resolution of panchromatic images and polarimetric synthetic aperture radar (PolSAR) data
- A novel dual-domain data fusion method is explored by combining spherically invariant random vector (SIRV) model with a novel generalized adaptive linear combination approximation (GALCA) technology
- Gaofen (GF)-2, 3 and Radarsat-2 data are used

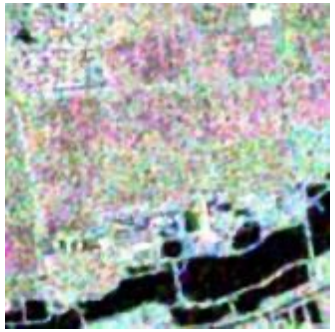

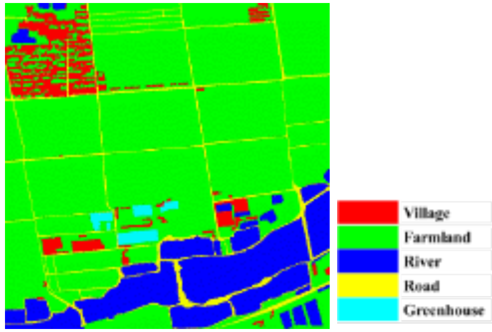

Ref: Liu et al. (2022)

Fusion of PolSAR & pan. images 2

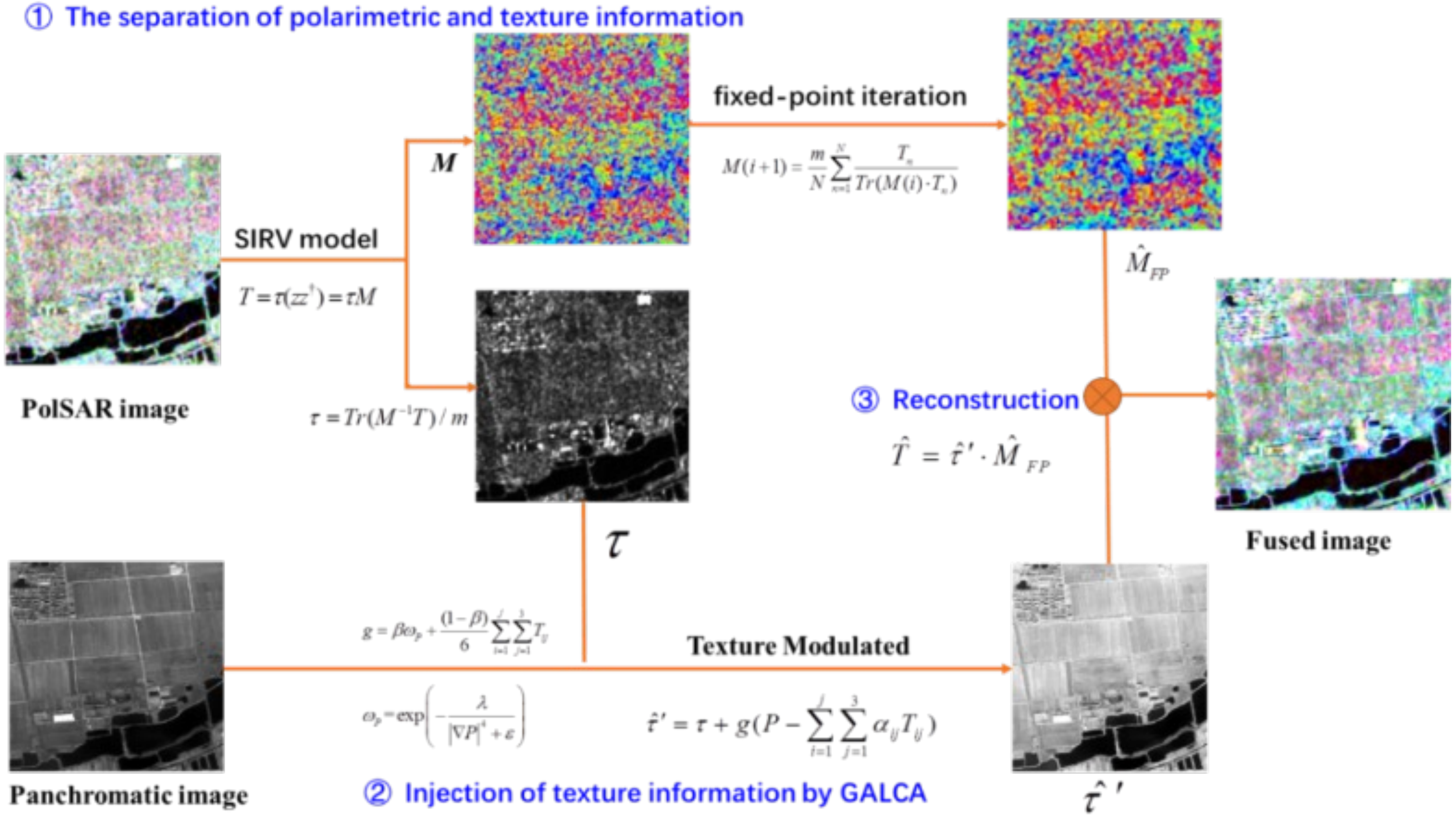

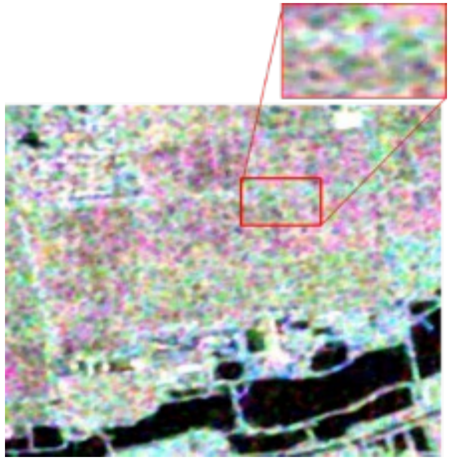

PauliRGB of original PolSAR image

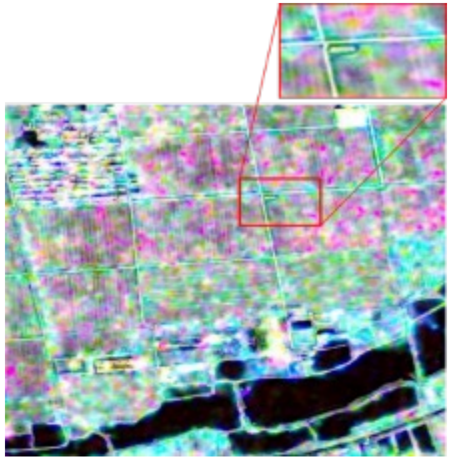

PauliRGB of fused PolSAR image

Results show that this can significantly improve spatial resolutions of PolSAR image while preserving polarimetric information.

Ref: Liu et al. (2022)

UAV & Satellite Hyperspectral LAI 1

Using UAV hyperspectral data to estimate LAI

- Spectral resolution of 4 nm in the range of 450-950 nm
- All bands were evaluated and the optimal bands were selected based on multiple methods to construct new two-band vegetation indexes
- Correlation between LAI and the proposed two-band vegetation indexes was compared and analyzed, which provide the confidence of further developing LAI estimation approaches based on the SVR, PLSR and RFR
- The proposed vegetation indices can be easily understood and physically explained, as well as with strong applicability and low computational cost

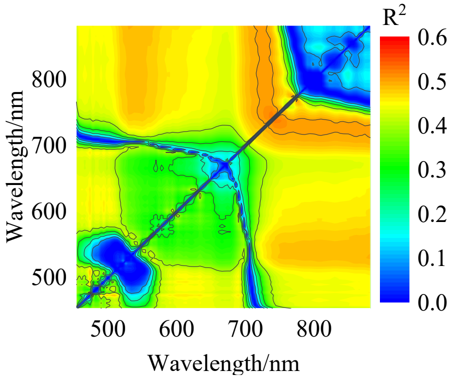

R^2 between LAI and NDSI

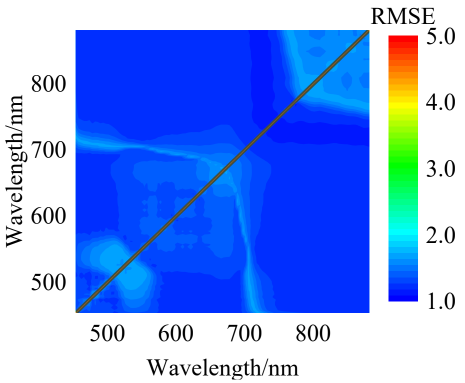

RMSE between LAI and NDSI

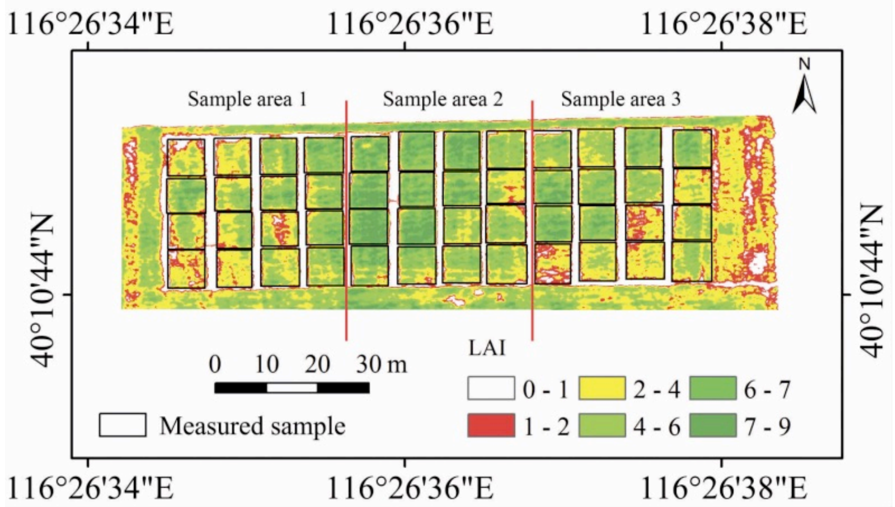

Ref: Kong et al. (2022)

UAV & Satellite Hyperspectral LAI 2

LAI estimation by a hybrid inversion strategy based on PROBA-CHRIS data

Ref: Liang et al. (2020,2021)

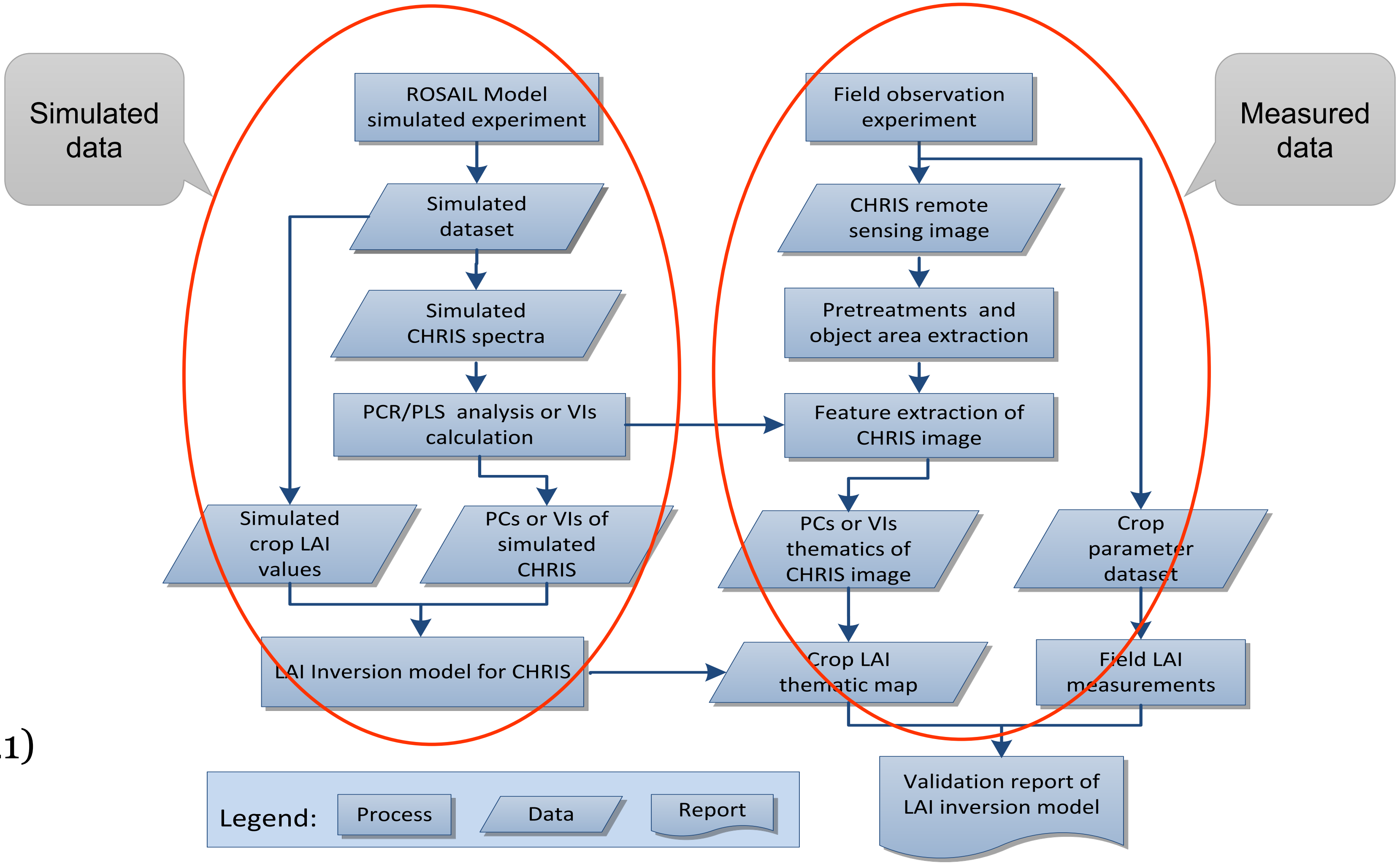

Flow chart of vegetation LAI remote sensing estimation based on integrated inversion strategy

UAV & Satellite Hyperspectral LAI 3

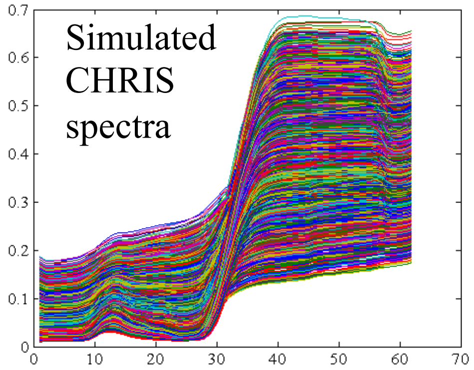

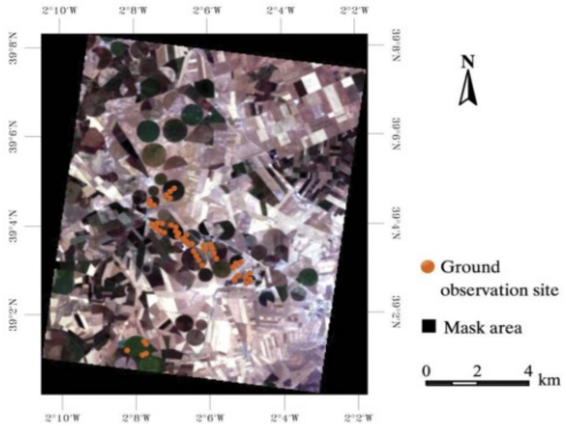

CHRIS image of study area

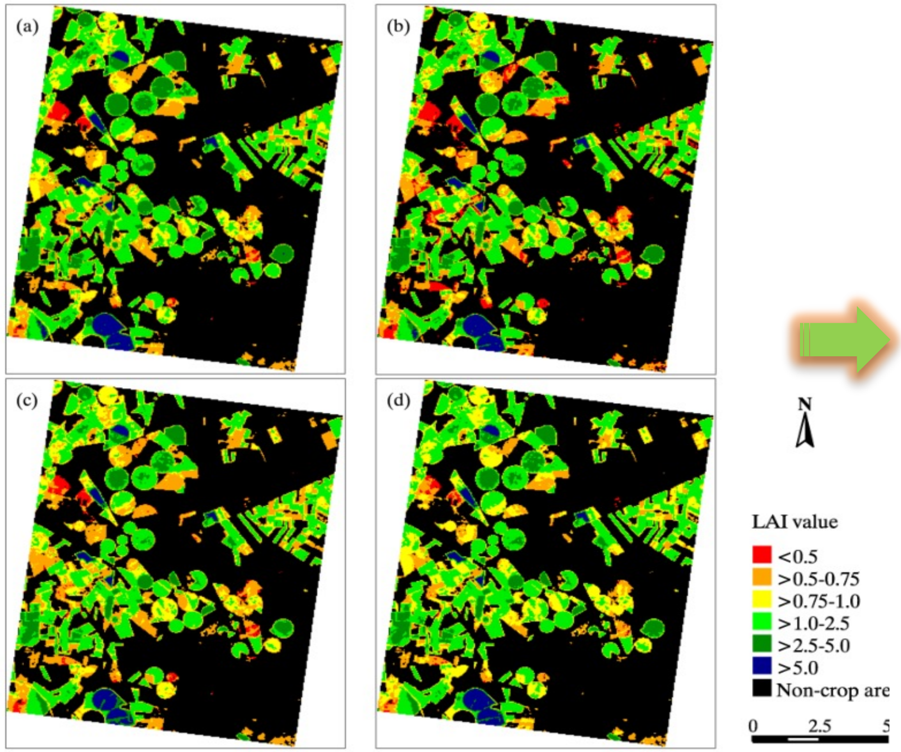

Spatial distribution map of the crop LAI predicted from the CHRIS remote sensing image and various RFR models in Sentinel-3 Experiment: (a) Specific2_PLS_RFR, (b) Specific1_PLS_RFR, (c) Generic_PLS_RFR , (d) Specific2 _OSAVI_RFR.

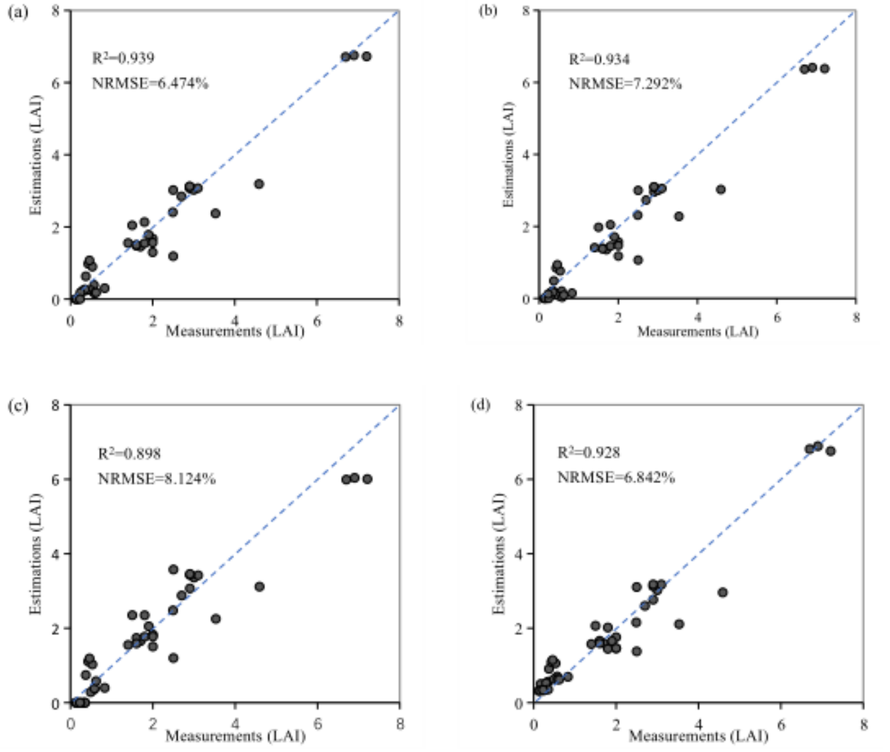

Ground-measured LAI versus the LAI estimated from the RFR inversion model in the Sentinel-3 Experiment: (a) Specific2_PLS_RFR, (b) Specific1_PLS_RFR, (c) Generic1_PLS_RFR, and (d) Specific2 _OSAVI_RFR.

Ref: Liang et al. (2020,2021)

PLMR Soil Moisture estimation

- A Bayesian probabilistic inversion algorithm can simultaneously estimate SM, surface roughness, and vegetation optical depth data and, to quantify the uncertainty in the inversion.
- Five comprehensive metrics were newly introduced into Bayesian posterior distributions of SM retrievals to indicate the performance of a retrieval algorithm
- Different combinations of polarizations and incidence angles of airborne polarimetric L-band multibeam radiometer (PLMR) observations as retrieval attempts were performed and the retrieved results were validated against multiscale ground-based measurements.

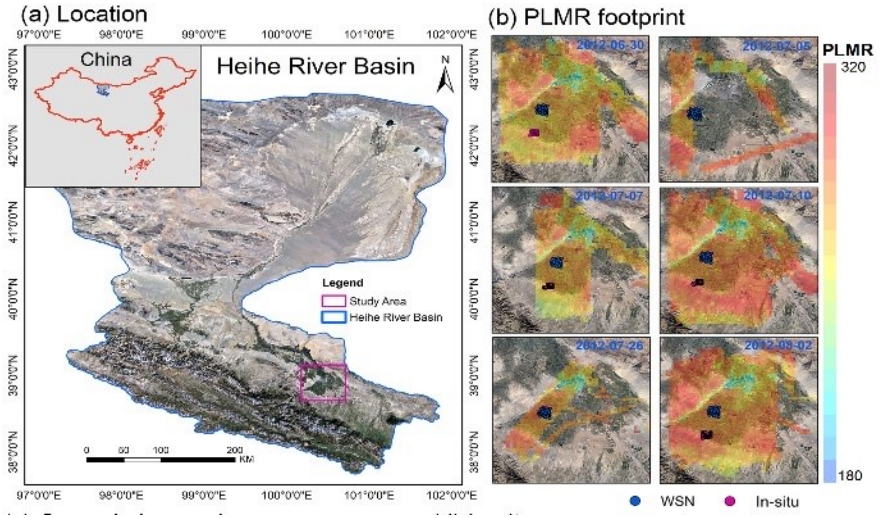

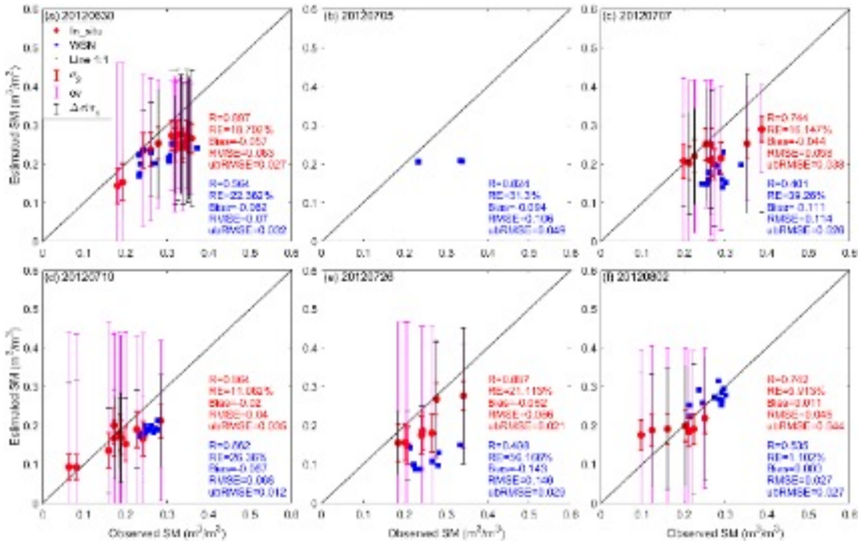

Ref: Ma et al. (2022)

Drought events monitoring 1

Analysis of drought occurrence frequency and change trend in China using long time series VCI, TVDI index products and meteorological data

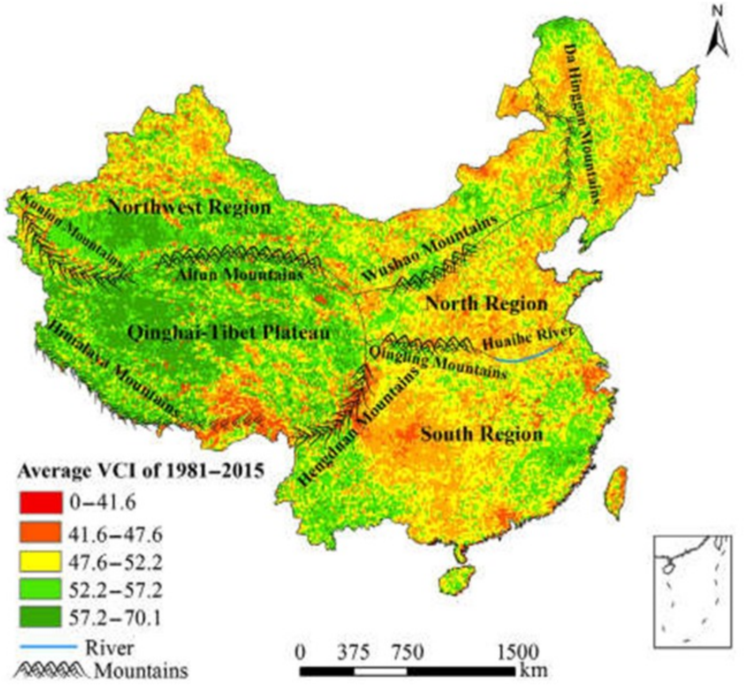

Fig. 1. Overview of the study area. The background is the average vegetation condition index (VCI) value from 1981 to 2015.

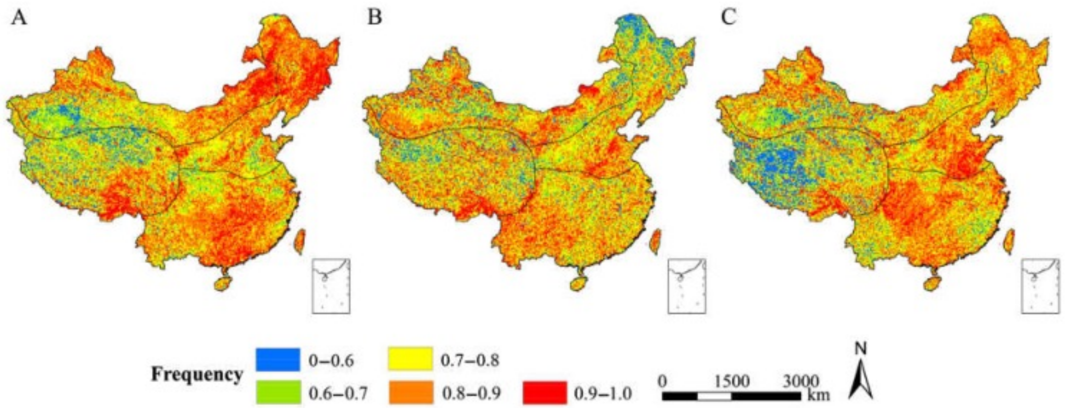

Fig. 2. Spatial distribution of the total drought occurrence frequencies in China for (A) spring, (B) summer, and (C) autumn.

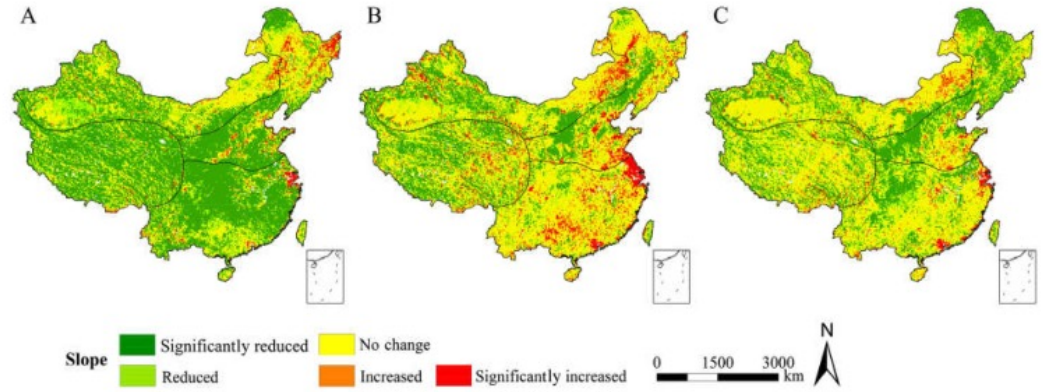

Fig. 4. Vegetation condition index trends from 1981 to 2015 in China for the (A) spring, (B) summer, and (C) autumn.

Ref: Liang et al. (2021)

Drought events monitoring 2

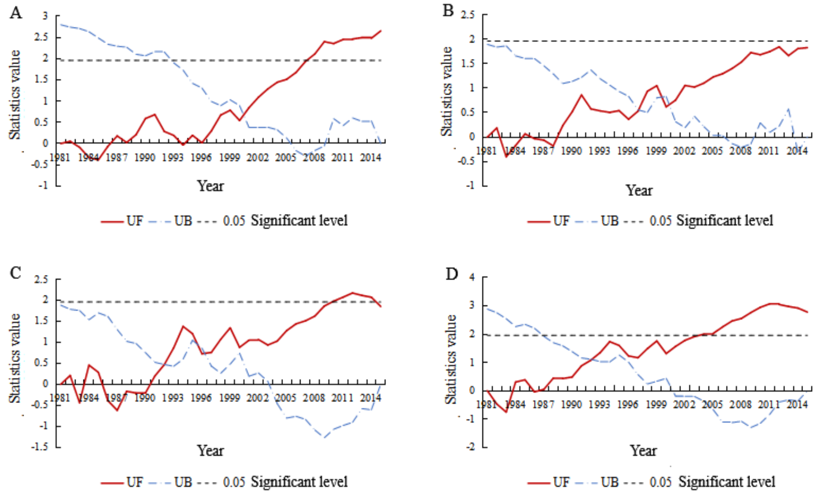

Mann-Kendall mutation analysis results of VCI time series for various regions of China

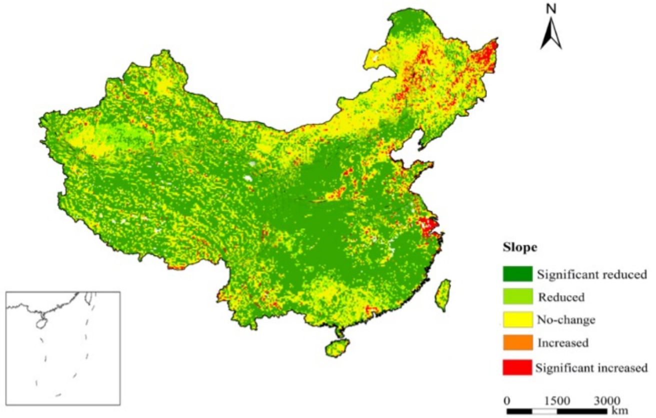

Slope trend of the average VCI in spring from 1981-2015 in China

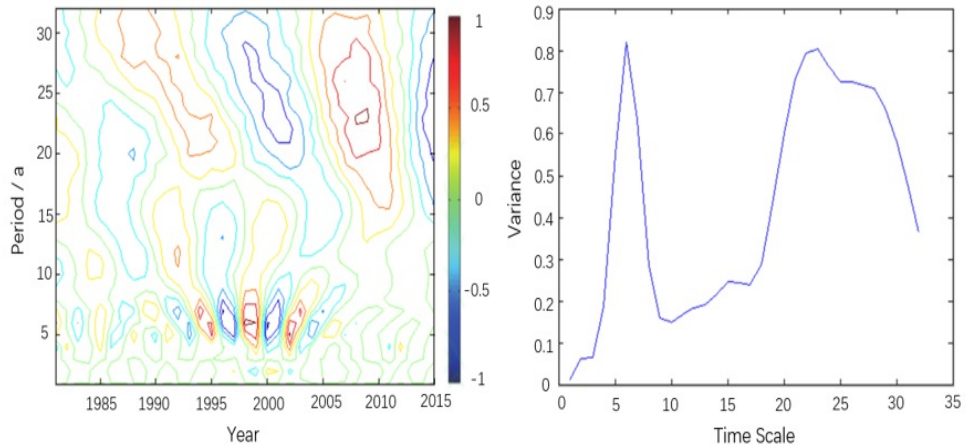

Wavelet time series analysis of spring VCI in China, 1981-2015.

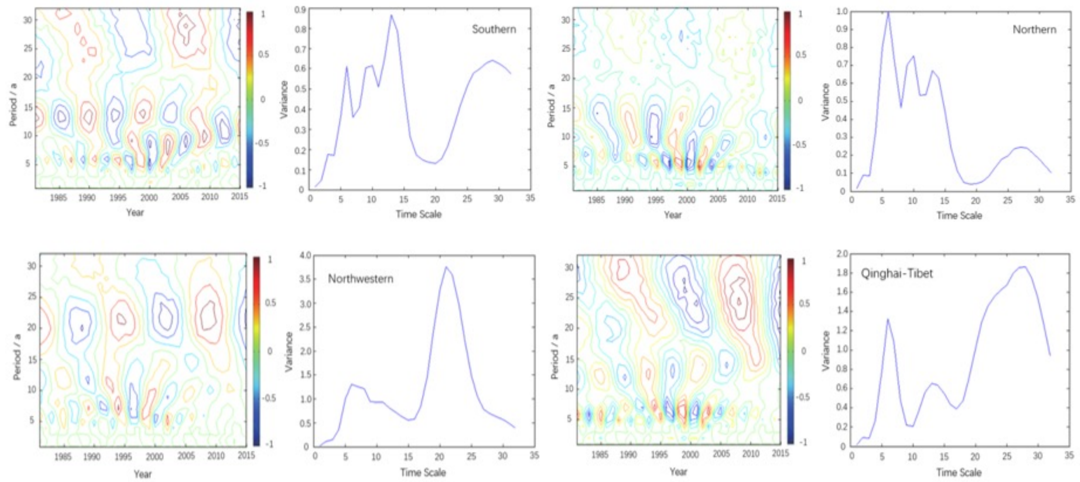

Spring VCI wavelet time series analysis maps for the southern (A), northern (B), northwestern (C) and Qinghai-Tibet (D) regions of China.

Ref: Liang et al. (2021)

Soil organic carbon 1

Mapping the soil organic carbon (SOC) changes in China from 1982 to 2019

Soil data
4695 soil sites
Sampled 1980s-2010s

Covariates
Multi-source
Represent key controls
Remote sensing provides temporal products

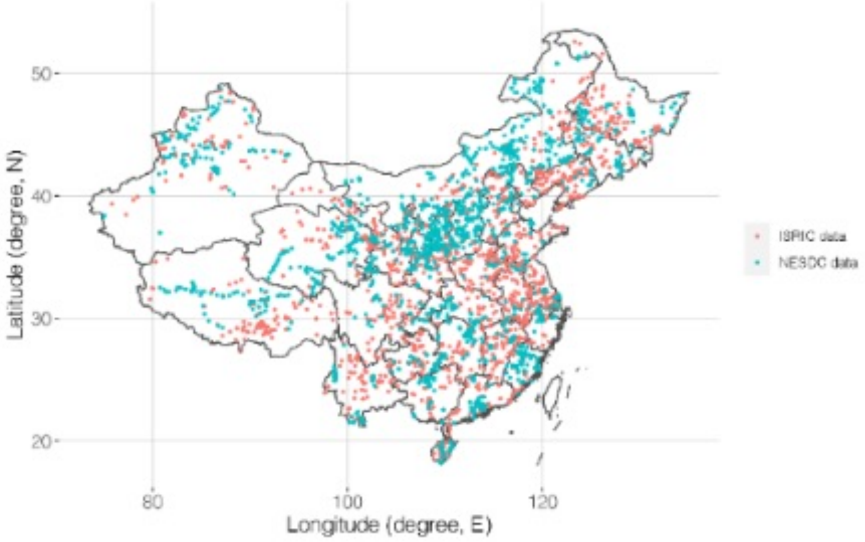

Spatial modeling
A machine learning-based statistical model Cubist

Model projection
Updating dynamic variables in the model

Category	Source	Resolution	Temporal scale
Terrain	SRTM Digital Elevation Model Data Version 4	Raster, 90 m	Stable
Climate	TerraClimate	Raster, ~4 km	Monthly, 1982-2019
Vegetation	GIMMS NDVI3g v1	Raster, ~8 km	twice a month, 1982-2015
	MOD13A2 NDVI	Raster, 1 km	16-day, 2016-2019
Soil	SoilGrids	Raster, 1 km	Stable
Parent material		Polygon, 1: 1,000,000 scale	Stable
Human activities	the Resource and Environment Science and Data Center of the Chinese Academy of Sciences	Raster, 1 km	for years 1980, 1990, 1995, 2000, 2005, 2010, 2015, and 2018
		Polygon	Dynamic
Others		Raster, 1 km	Stable
			Dynamic

Ref: Yang et al. (2022)

Soil organic carbon 2

Soil organic carbon density dataset for China from 1982–2019

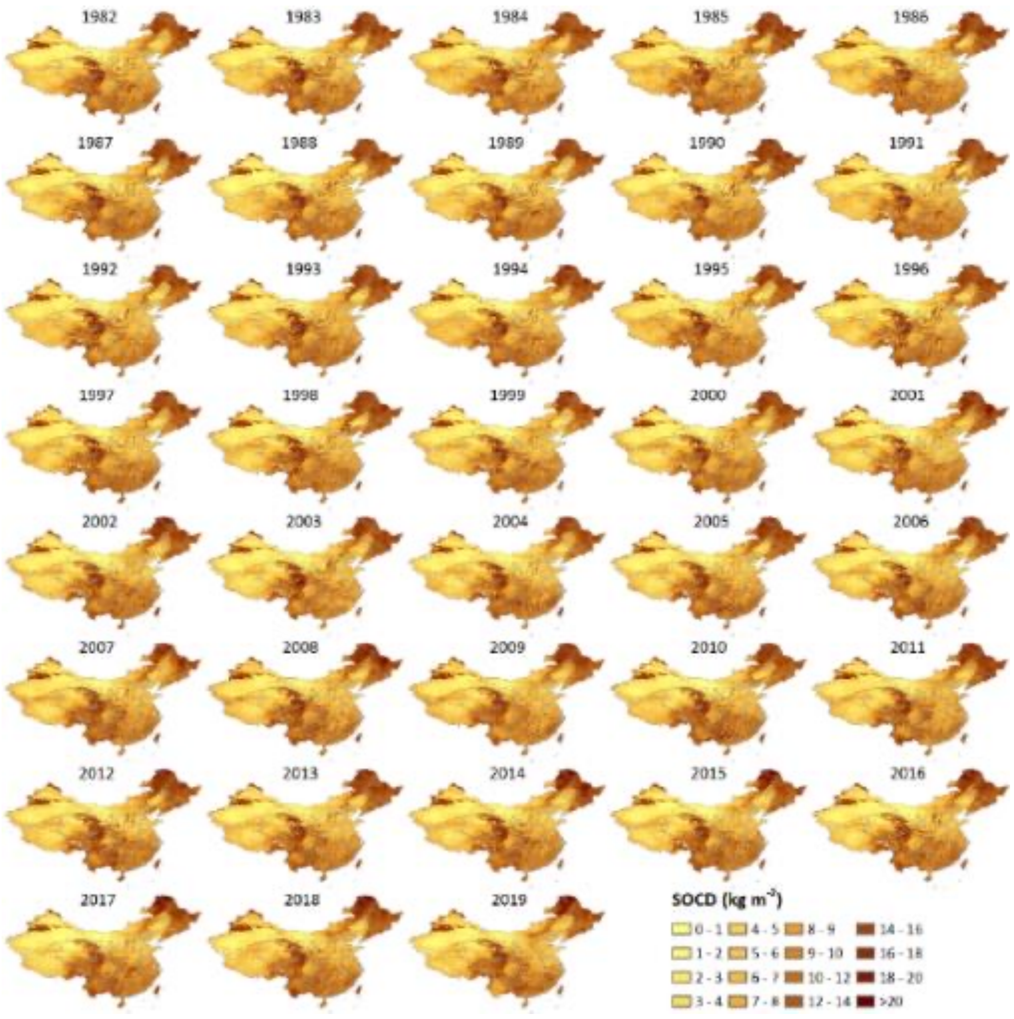

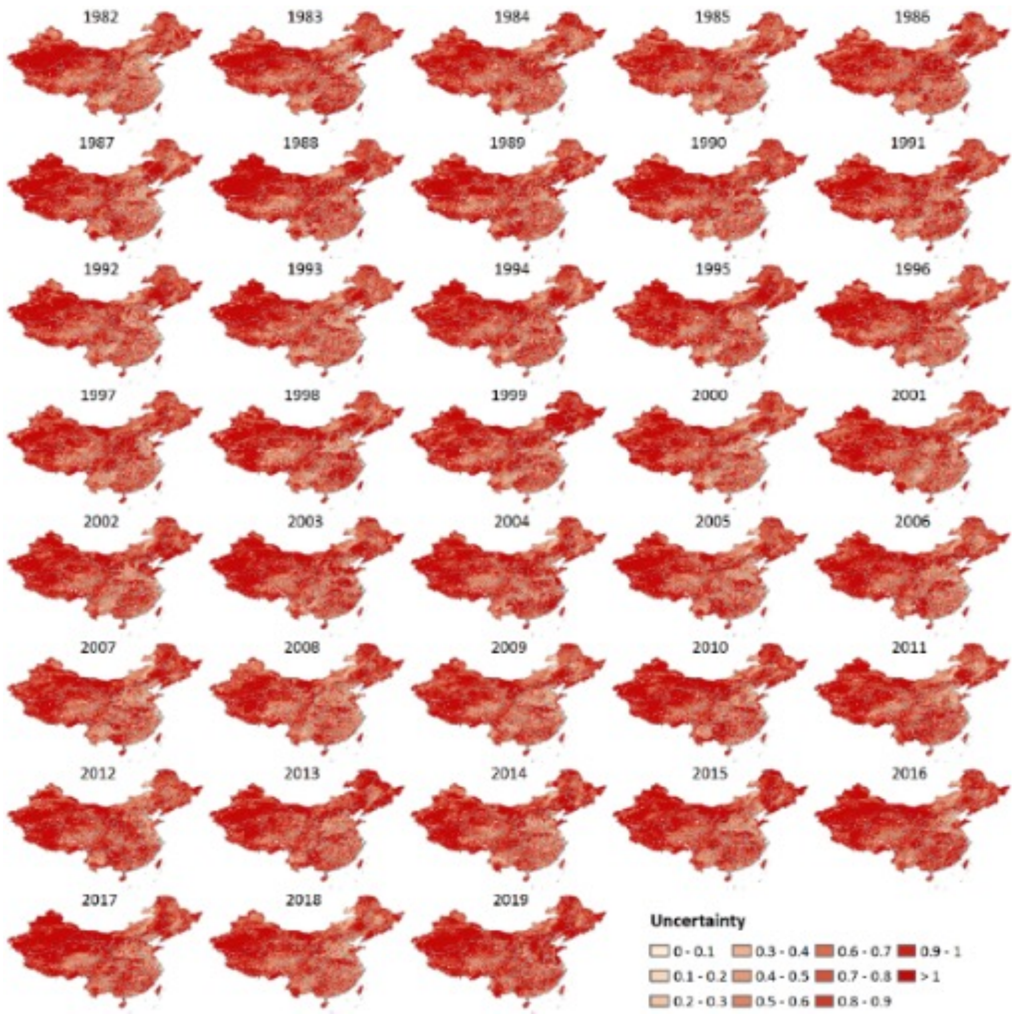

Ref: Yang et al. (2022)

Soil organic carbon 3

Further, key driving factors to the SOC variations are analyzed.

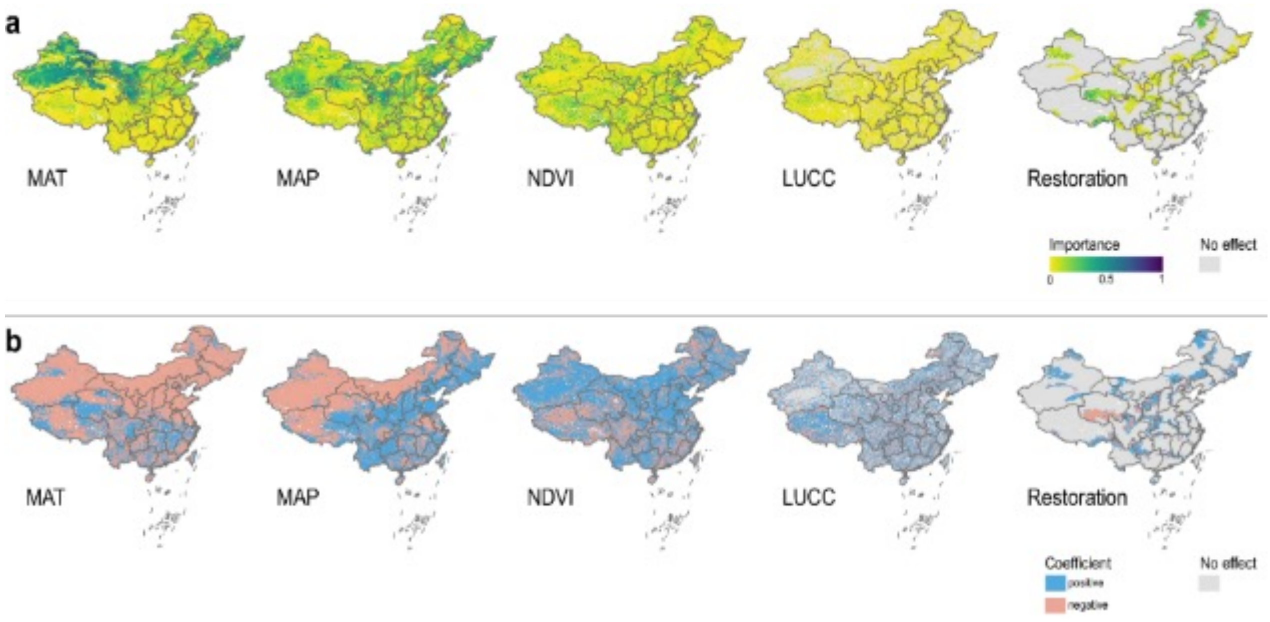

Spatial pattern of the controls of the soil organic carbon density (SOCD) change in 1982 and 2019

- The annual SOC distribution at a depth of 0-100 cm with 1 km spatial resolution between 1982 and 2019.
- The controlling factors included elements representing temperature, precipitation, vegetation, and human activities.
- The findings offer a unique view of the diverse spatial patterns and controls of long-term SOC changes in China and enables spatially explicit assessments of soil carbon dynamics, which can be beneficial to policy making in relation to carbon offset activities.

Ref: Yang et al. (2023)

Large scale NEP 1

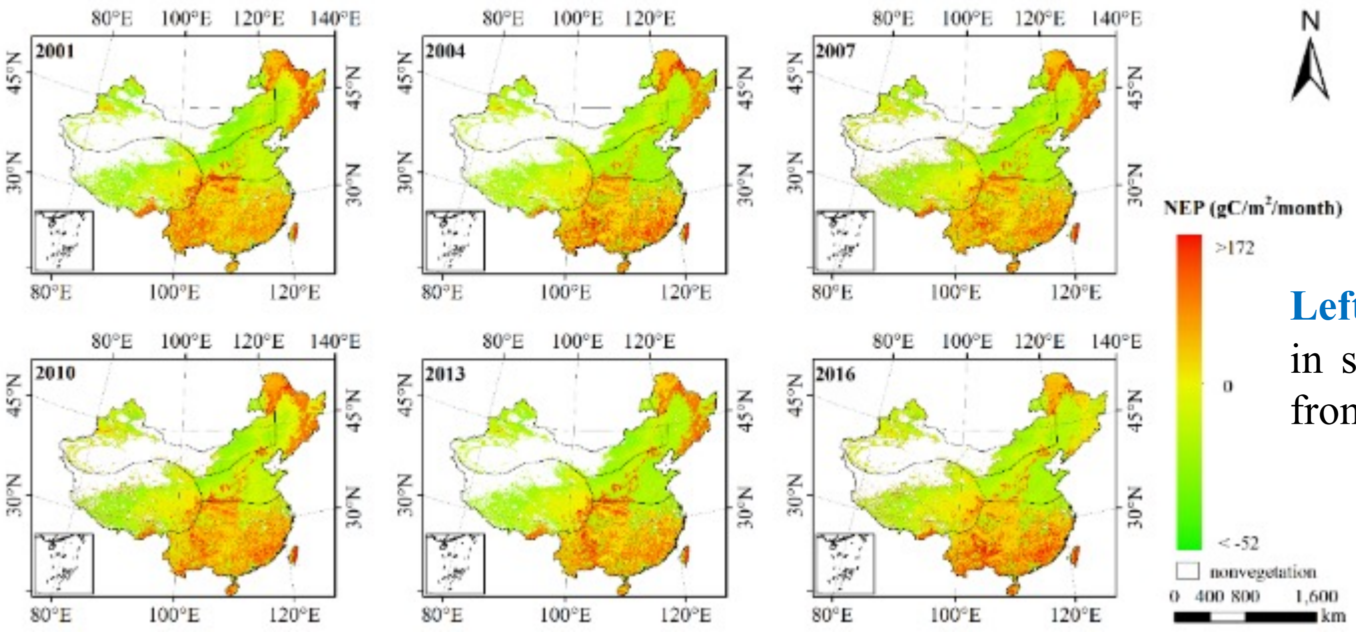

Left: Average NEP in summer of China from 2001 to 2016

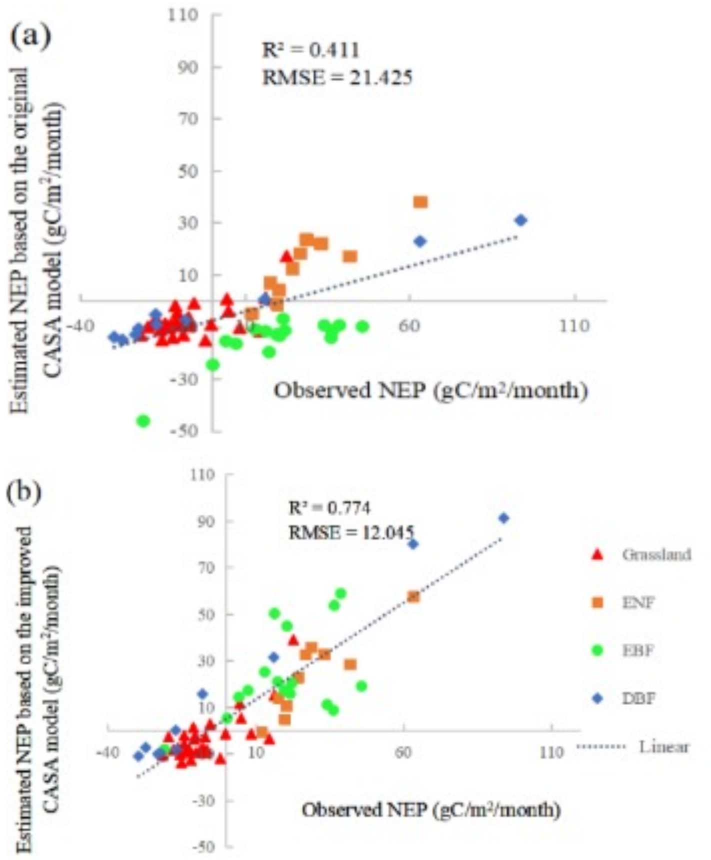

The observed NEP VS the estimated NEP based on the CASA model. (a) ε_{max} using vegetation classification; (b) ε_{max} of fixed value 0.389 ($gC \cdot MJ^{-1}$)

- NEP was estimated by coupling the optimized CASA model, the geostatistical model of soil respiration, and the soil respiration-soil heterotrophic respiration relationship.
- Results improved remarkably, with an increase of R^2 from 0.411 to 0.774 and a decrease of RMSE from 21.425 $gC \cdot m^{-2} \cdot month^{-1}$ to 12.045 $gC \cdot m^{-2} \cdot month^{-1}$.

Ref: Liang et al. (2022)

Large scale NEP 2

- Similarly, by optimizing the parameters optimum temperature and ε_{max}, the modified CASA model was employed to obtain terrestrial ecosystem NPP and NEP over Europe.
- The detailed trend of monthly changed NEP in each region can be analyzed, while the overall trend was annually positive.

Vegetation Types	abbreviation	ε_{max}(gC·MJ^{-1})
Evergreen Needleleaf Forests	ENF	1.730
Evergreen Broadleaf Forests	EBF	1.430
Deciduous Needleleaf Forests	DNF	1.730
Deciduous Broadleaf Forests	DBF	2.110
Mixed Forests	MF	1.550
Closed Shrublands	CSH	1.530
Open Shrublands	OSH	1.530
Grasslands	GRA	1.530
Wetlands	WET	1.530
Croplands	CRO	1.790

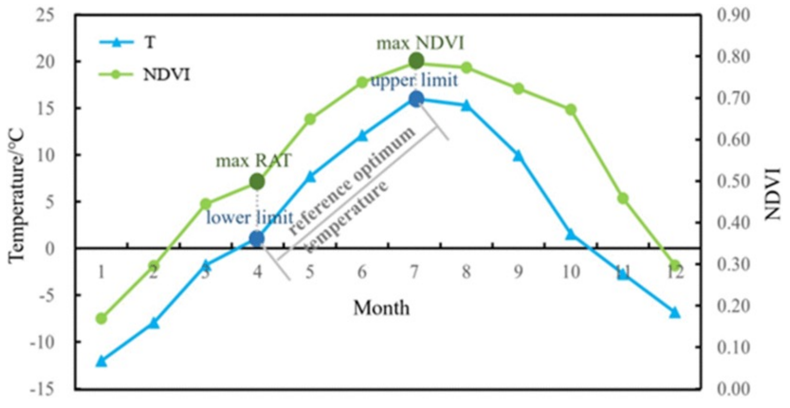

Annual variation chart of monthly average temperature and monthly average NDVI.

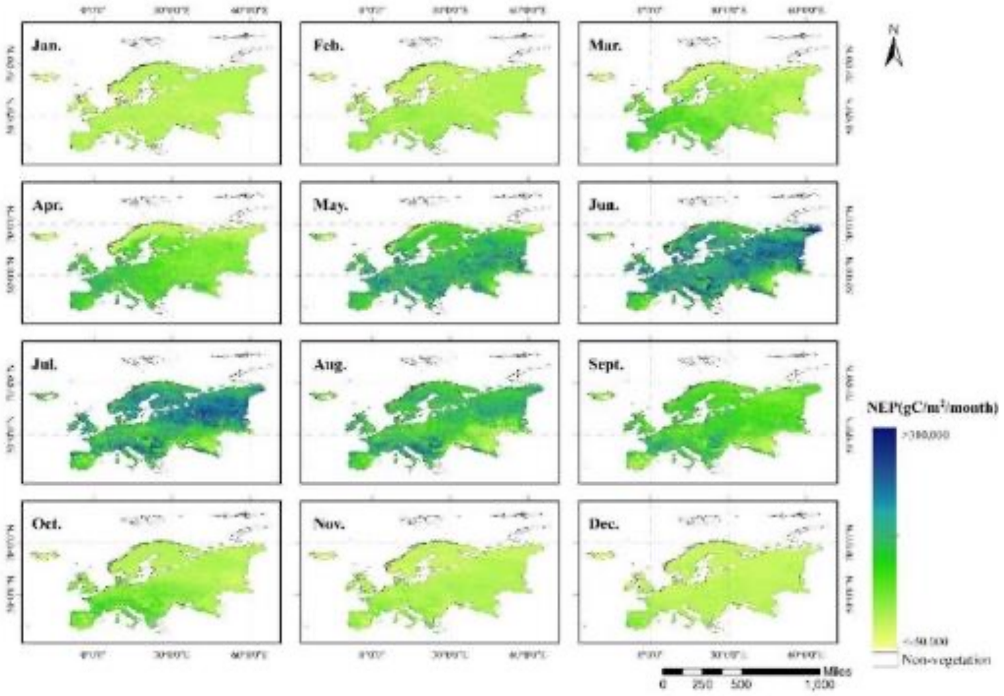

Spatiotemporal distribution of monthly NEP in Europe in 2014

Ref: Qiu et al. (2023)

3. Conclusion and outlook

- Systematic exploitation of multi-source and multi-scale remote sensing observations through modeling can provide valuable opportunity to gain knowledge about agroecosystem processes.
- Joint publication submitted to Geo-spatial Information Science (GSIS), Current status is "Decision Pending" after 1st round of revision.
- Next, near-real-time estimation of essential variables to timely inform crop growth models will be further developed.
- To combine the different variable types and strengthen the synergies from remote sensing monitoring to modeling, agroecosystem functioning and the feedback in the soil-vegetation-lower atmosphere will be investigated with the data assimilation framework.

4. Young scientists

- Early-career scientists, PhD and Master students are members of the team to contribute to algorithm and model development, satellite data processing and analysis, and field campaigns.
- The education of young scientists in the field of remote sensing of agriculture to multiply their EO expertise in their further career at different stakeholders.

- European side: Bagher Bayat, Jordan Steven Bates, David Mengen, Wenqin Huang, Shirin Moradi, Yuquan Qu, Rahul Raj, Visakh Sivaprasad, Xuerui Guo
- Chinese side: Wensong Liu, Lu Xu, Jiangguo Li, Renmin Yang, Siyi Qiu, Yanyan Shi, Di Geng, Juan Yan, Ting Huang, Jingjing Xu, Xin Liu, Peilin Yin

European Young scientists contributions in Dragon 5

Name	Institution	Poster title	Contribution including period of research
Bagher Bayat	Forschungszentrum Juelich (IBG-3)	Agricultural Water Stress Monitoring by MSG-SEVIRI ET Observations Across Europe: a Comprehensive Accuracy Assessment and an ESI-based Water Stress Product	Remote sensing of water stress (2004-2018)

Chinese Young scientists contributions in Dragon 5

Name	Institution	Poster title	Contribution including period of research
LI Jinzhi	JSNU	Remote sensing monitoring and evaluation of ecological environment of Guangyuan City in Mountain-Basin Transition Zone	Remote sensing for ecological and environmental monitoring, especially for water quality
SHI Jin	JSNU	A remote sensing extraction method for garlic distribution in Pizhou City using GEE cloud platform	Remote sensing for ecological and environmental monitoring, especially for plant type
SUN Chen	JSNU	Spatial-temporal variation analysis and prediction of carbon storage in urban ecosystems based on PLUS-InVEST model: A case study of Xuzhou	Remote sensing for ecological and environmental monitoring, especially for carbon storage
WANG Qianjie	JSNU	Insights into the sustainability and driving mechanism of NPP of terrestrial vegetation in Africa	Remote sensing for ecological and environmental monitoring, especially for carbon storage

5. EO Data Delivery

Data access (list all missions and issues if any). NB. in the tables please insert cumulative figures (since July 2020) for no. of scenes of high bit rate data (e.g. S1 100 scenes). If data delivery is low bit rate by ftp, insert “ftp”

ESA /Copernicus Missions	No. Scenes
1. Sentinel-1	~50
2. Sentinel-2	~50
3.	
4.	
5.	
6.	
Total:	~100
Issues:	

ESA Third Party Missions	No. Scenes
1. PROBA-CHRIS	~10
2. MSG-SEVIRI	~10000
3. PlanetSCOPE	~20
4. ALOS-2	~50
5.	
6.	
Total:	10K+
Issues:	

Chinese EO data	No. Scenes
1. GF series	~100
2.	
3.	
4.	
5.	
6.	
Total:	~100
Issues:	

Thank you !

Dr. Liang Liang（梁亮）
School of geography, geomatics and planning
Jiangsu Normal University, Xuzhou 221116, China
liang_rs@jsnu.edu.cn

Dr. Carsten Montzka
Forschungszentrum Jülich GmbH, IBG-3,
Leo-Brandt-Strasse, 52428 Jülich, Germany
c.montzka@fz-juelich.de